Supporting Information

Tuning mesomorphic, spectral and nonlinear optical behavior in chalcogenophene triads: the role of oxygen, sulfur, and selenium

Natan Rychłowicz*, Jakub Karcz, Alina Szukalska, Rafał Wysokiński, Bouchta Sahraoui, Jarosław Myśliwiec, Przemysław Kula

[1]Institute of Chemistry, Faculty of Advanced Technology and Chemistry, Military University of Technology, 00-908 Warsaw, Poland
[2]Soft Matter Optics Group, Wroclaw University of Science and Technology, Wyb. Wyspiańskiego 27, 50-370 Wroclaw, Poland
[3]Faculty of Chemistry, Wroclaw University of Science and Technology, Wyb. Wyspiańskiego 27,50-370 Wroclaw, Poland
[4]Univ Angers, LPHIA, SFR MATRIX, F-49000 Angers, France

* Corresponding: Natan Rychłowicz natan.rychlowicz@wat.edu.pl

Table of contents

Experimental details and methods

General remarks

All reagents were purchased from commercial suppliers and used without further purification. Tetrahydrofuran used in synthesis was dried with sodium prior to usage. Purification of products was performed with column chromatography using silica gel (100–200 mesh). Synthesis progress and the purity of the synthesized compounds were determined using a SHIMADZU GCMS-QP2010S (Shimadzu, Kyoto, Japan) series gas chromatograph equipped with a quadrupole mass analyzer MS(EI), high-performance liquid chromatography HPLC-PDA-MS (APCI-ESI dual source), Shimadzu LCMS 2010 EV (Shimadzu, Kyoto, Japan) equipped with a polychromatic UV–VIS detector (Shimadzu, Kyoto, Japan) and by thin-layer chromatography (silica gel 60 with fluorescent indicator on aluminum, Macherey-Nagel, Germany). ^{1}H and ^{13}C NMR spectra in THF-d_8 were collected using a Bruker model Avance III spectrometer (Bruker, Billerica, MA, USA). For PES-5O and PES-5S only ^{1}H NMR spectra were collected using nitrobenzene-d_5/DMSO-d_6 mixture as a solvent due to their poor solubility in other deuterated solvents.

Absorption spectroscopy

Absorption spectra were recorded with a UV-Vis-NIR spectrometer Shimadzu UV-3600 (Shimadzu, Kyoto, Japan). Solutions were prepared in spectrally pure DCM (Thermo Fisher Scientific, Waltham, MA, USA) with concentration of approx. $1x10^{-5}$ M.

Fluorescence spectroscopy

Spectrofluorimetric measurements were recorded on Edinburgh Instruments FS5 spectrofluorometer (Livingston, UK) from solution in transmissive mode. Compounds were dissolved in spectrally pure DCM (Thermo Fisher Scientific, Waltham, MA, USA), and spectra were collected from solution of concentration approx. $1x10^{-5}$ M. Quantum yield of fluorescence measurements were performed with calibrated integrating sphere (SC-30 module for FS5 spectrofluorometer) in quartz cuvettes with optical path of 1cm from solutions in DCM with concentration adjusted in a way that its absorbance was 0.1±0.01.

Polarization optical microscopy (POM) and differential scanning calorimetry (DSC)

The phase transition temperatures were determined by polarizing optical microscopy (POM) with an OLYMPUS BX51 (Olympus, Shinjuku, Tokyo, Japan) equipped with a Linkam hot stage THMS-600 (Linkam Scientific Instruments Ltd., Tadworth, UK). Precise temperature and enthalpy data were collected with differential scanning calorimeter DSC 204 F1 Phoenix instrument (Netzsch, Selb, Germany) with the scanning rate of 2 K min^{-1} on both the heating and cooling cycles with the 5-minute isothermal step between cycles.

Computational Details

All DFT and TD-DFT calculations were performed using the Gaussian 16 (C.01)[1] suits of programs. The geometrical and vibrational parameters of the ground state were determined with DFT/MN15 and the 6-31+G(d) atomic basis set, in the presence of the solvent (dichloromethane), exploiting the Polarizable Continuum Model (PCM). All presented structures correspond to the true minima of the potential energy surface (no imaginary frequencies were found). The

transition energies between the S0 and S1 states have been determined at the TD-DFT level of theory.
Time-dependent density functional theory (TD-DFT) was also employed to compute the second hyperpolarizabilities with the CAM-B3LYP[2] exchange–correlation (XC) functional and the 6-311G basis set. CAM-B3LYP has been reported to deliver good accuracy in predicting the NLO properties[3]. The calculations were performed with the Dalton software[4,5] considering the frequently employed optical perturbation at 1064 nm wavelength.

Sample preparation THG measurements

For the Third Harmonic Generation (THG) experiment, the thin-film samples were prepared following a defined protocol. Firstly, a 5% solution containing the optically passive PMMA polymer (Sigma–Aldrich®) was formulated by dissolving it in dichloromethane. Then, each dye in the form of powder was introduced to the solution, to achieve a precise 5% dry weight-to-weight ratio between the chromophore and PMMA mass. Subsequently, the prepared solutions were utilized to create thin films via the Spin-Coating method. A single cycle lasting 45 seconds at a speed of 1000 rpm was used to deposit 300 µL of solution onto glass substrates, providing thin films measuring less than 3.5 microns in thickness (see **Table 5** in main text).

NLO spectroscopic measurements

The absorbance spectra of dyes embedded in a PMMA matrix were measured at room temperature using a UV-1800 Shimadzu (Shimadzu, Kyoto, Japan) spectrophotometer.
To acquire and analyse the nonlinear optical (NLO), THG response, the Maker Fringes method was employed, utilizing a picosecond pulsed Nd:YAG laser (EKSPLA, PL2250 Series) emitting a 1064 nm fundamental wavelength, with a pulse duration of 30 ps, and a repetition frequency of 10 Hz. The laser beam, directed towards the sample mounted on a rotating table, passed through an optical system comprising a polarizer, a half-wave plate, a filter for second harmonic radiation separation, and a focusing lens. The rotating table allowed for sample positioning at angles ranging from +60° to -60° relative to the normal. Grey and interference filters regulated beam intensity before analysis via computer software, with real-time monitoring facilitated by an oscilloscope. Laser energy was 100 µJ (measured using a Coherent - Field Max II® power meter). Consistent thickness was observed across multiple regions of the thin films, confirming the high quality of the deposition process using a profilometer (Dektak 6M, Veeco).

When analyzing the intensity of the THG signal as a function of angle, a characteristic pattern known as the Maker Fringes emerges. This pattern arises from the interference between the generated third harmonic and the fundamental wave as they propagate through NLO material. Varying the angle of incidence changes the relative phase between these waves, producing constructive and destructive interference that leads to an oscillatory THG intensity profile. It typically displays two peaks around ±10°, symmetrically positioned relative to each other, and such proportional angular distribution of the Maker Fringes suggests a uniform and balanced response of the material to the incident optical field. This arrangement can be compared to a reference material like Silica.

THG calculations – Kubodera-Kobayashi Model

For the calculation of the materials' third-order nonlinear susceptibility ($\chi^{(3)}$), the comparative Kubodera-Kobayashi model[6,7] was applied. $\chi^{(3)}$ quantifies the strength of the NLO response, crucial for understanding and characterizing the efficiency of THG processes[8]. Due to the significant absorbance at 355 nm, the estimation of $\chi^{(3)}$ incorporated absorption coefficient α, and the calculations followed a specified formula:

$$\chi^{(3)} = \chi^{(3)}_{silica}\left(\frac{2}{\pi}\right)\left(\frac{L^{coh}_{silica}}{d}\right)\left(\frac{\frac{\alpha d}{2}}{1-\exp\left(-\frac{\alpha d}{2}\right)}\right)\left(\frac{I^{3\omega}}{I^{3\omega}_{Silica}}\right)^{\frac{1}{2}}$$

Where:

$\chi^{(3)}_{silica}$ = $2.0 \cdot 10^{-22}$ [m^2/V^2] [9]

L^{coh}_{silica} = 6.7 [μm]; a coherence Silica length, calculated using the following equation:

$$L^{coh}_{Silica} = \frac{\lambda}{6 \cdot |n_{3\omega} - n_{\omega}|}$$

$n_{3\omega}$, and n_{ω} = demonstrates the refractive index of the material at the tripled in frequency (355 nm, 1.4761), and at fundamental (1064 nm, 1.4496) wavelengths, respectively.

d = sample thickness [μm]

α = absorption coefficient [cm^{-1}]

$I^{3\omega}$ and $I^{3\omega}_{silica}$ are the maximum THG intensities of the sample and Silica obtained from the measurement [Arb. Un.].

Synthetic procedures

2,2'-bifuran

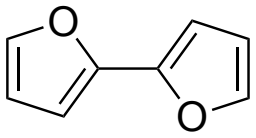

To a stirred solution of furan (34g, 0.5mol) and dry THF (300ml) at -10°C, the solution of n-butyllithium in hexanes (210ml, 0.525mol, c=2.5M) was added dropwise. After addition, solution was stirred at -10°C for 1,5h. Then it was cooled to -30°C and the solid $CuCl_2$ (67.2g, 0.5mol) was added portion wise while keeping the temperature below -20°C. Next, the reaction mixture was warmed to room temperature followed by addition of hydrochloric acid. The mixture was transferred to separatory funnel and extracted with DCM. Organic phase was dried over $MgSO_4$ and concentrated under vacuo. Then the product was filtered through silica gel using hexane as the eluent and concentrated under vacuo to give yellow liquid.
Yield: 18.12g (54%).
Purity: 94.5%.
MS(EI) m/z: 134; 105; 95; 78; 67; 51; 39; 29

5,5'-dibromo-2,2'-bifuran

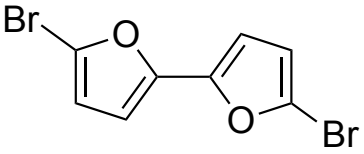

To a stirred solution of 2,2'-bifuran (3g, 0.0224mol) in benzene (50ml), N-bromosuccinimide (7.97g, 0.0448mol) was added portion wise at room temperature. After addition, the solution was stirred at RT for 15 minutes and followed by addition of water. Then the phases were separated. Organic phase was dried over $MgSO_4$ and concentrated under vacuo. The product was purified by column chromatography using hexane as the eluent to give pale yellow crystals. The reaction was repeated before every Sonogashira coupling reaction due to the photodegradation of the 5,5'-dibromo-2,2'-bifuran.
Yield: 6.17g (94.3%).
Purity: 97,6%.
MS(EI) m/z: 292; 211; 183; 155; 132; 117; 104; 76; 63; 50

2,5-dibromothiophene

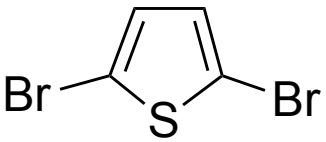

To the stirred solution of thiophene (84g, 1mol), HBr (250ml) and diethyl ether (250ml) at -15°C, the mixture of Br_2 (320g, 2mol) and HBr (120ml) was added dropwise. After the addition the solution was warmed to room temperature. The mixture was transferred to separatory funnel, washed with H_2O and extracted with DCM. The organic phase was dried over $MgSO_4$ and concentrated under vacuo. The crude product was then purified by vacuum distillation.
Yield: 217.74g (90%).
Purity: 99.0%.
bp = 61°C (1.57 Torr)
MS(EI) m/z: 242; 163; 117; 82; 57; 28

5,5'-dibromo-2,2'-bithiophene

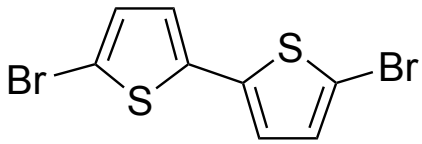

To a stirred solution of 2,5-dibromothiophene (30g, 0.124mol) and diethyl ether (500ml) at -70°C, the solution of n-butyllithium in hexanes (57ml, 0.14mol, c=2.5M) was added dropwise. After addition, solution was stirred at -70°C for 1h. Then solid $CuCl_2$ (50g, 0.372mol) was added portion wise. The reaction mixture was warmed to room temperature and poured on hydrochloric acid. The mixture was transferred to separatory funnel and extracted with DCM. The organic phase was washed with saturated sodium bicarbonate solution, dried over $MgSO_4$ and concentrated under vacuo. Crude product was purified by short path vacuum distillation using a Kugelrohr distillator.

Yield: 11,5g (57.2%)

Purity 98,7%

mp = 149.5°C

MS(EI) m/z: 324; 245; 201; 164; 120; 82; 69; 45; 28

2,2'-Biselenophene

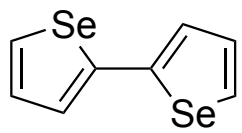

Selenophene (5.00 g, 38.16 mmol) was dissolved in anhydrous Et_2O (150 mL), and n-butyllithium (16.8 mL, 41.97 mmol) was added dropwise at room temperature. The reaction mixture was heated to reflux and maintained for 15 minutes. Afterward, it was cooled to room temperature and then further to -65°C. $CuCl_2$ (10.26 g, 76.3 mmol) was added in one portion, and the reaction was stirred at -65°C for 30 minutes. The mixture was then warmed to room temperature and quenched with diluted HCl solution. After extraction with DCM, the organic extracts were combined, washed with distilled water, dried over $MgSO_4$, and the solvent was evaporated using a rotary evaporator. The product was purified by short-path vacuum distillation using a Kugelrohr distillator.

Yield: 2.40g (48%).

Purity: 94.3%.

MS(EI) m/z: 262; 182; 169; 156; 141; 130; 117; 102; 89; 74; 63; 50; 39; 28

5,5'-Dibromo-2,2'-biselenophene

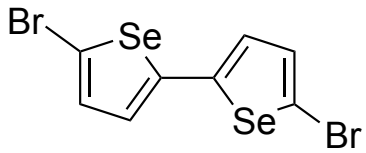

2,2'-Biselenophene (2.40 g, 9.23 mmol) was placed in a flask, followed by the addition of $CHCl_3$ (75 mL) and acetic acid (75 mL). N-Bromosuccinimide (3.61 g, 20.30 mmol) was then added, and the reaction mixture was stirred at room temperature for 72 hours. Upon completion, the reaction mixture was washed with distilled water, and the organic phase was dried over $MgSO_4$. The solvent was then evaporated using a rotary evaporator. The crude product was recrystallized from acetone.

Yield: 3.30g (86%).

Purity 95,8%.

MS(EI) m/z: 418; 339; 260; 234; 209; 180; 155; 129; 105; 74; 50; 28.

General procedure for Sonogashira coupling

Dibromobichalcogenophene, DBU (2eq.), TEA (2eq.) were put in flask and dissolved in toluene (100ml). Reaction was heated to reflux, degassed for 15 minutes, and corresponding acetylene (2,2eq) was added dropwise. Reaction was monitored with TLC, after completion was quenched with diluted HCl and mixture was filtered through cellulose pad. Organic layer was washed with distilled water, dried, solvent was evaporated. Final compounds were purified with heated column chromatography and recrystallized from ethanol or/and acetone.

5,5'-bis[(4-pentylphenyl)ethynyl]-2,2'-bifuran (PEF-5)

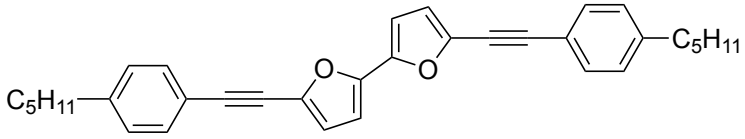

Yield: 56%
Purity 99.9% (HPLC-PDA)
MS(EI) m/z: 474; 445; 417; 389; 361; 332; 302; 276; 237; 209; 180; 152
^{1}H NMR (500MHz, THF-d$_8$) δ: 7.47 (d, *J*=8.24 Hz, 4 H); 7.25 (d, *J*=8.24 Hz, 4 H); 6.82 (d, *J*=3.36 Hz, 2 H); 6.79 (d, *J*=3.66 Hz, 2 H); 2.66 (t, *J*=7.63 Hz, 4 H); 1.67 (m, 4 H); 1.38 (m, 8 H); 0.94 (t, *J*=6.87 Hz, 6 H)
^{13}C NMR (125 MHz, THF-d$_8$) δ: 147.31; 145.02; 137.82; 132.04; 129.44; 120.26; 117.85; 108.26; 95.43; 79.45; 36.62; 32.38; 31.84; 23.39; 14.34

5,5'-bis[(4-(pentyloxy)phenyl)ethynyl]-2,2'-bifuran (PEF-5O)

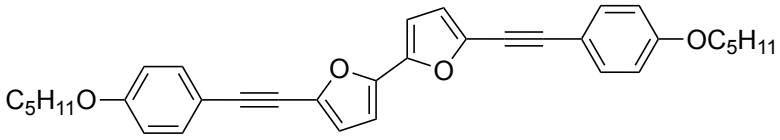

Yield: 45%
Purity 97.0% (HPLC-PDA)
MS(EI) m/z: 506; 435; 379; 365; 337; 308; 279; 252; 224; 200; 168; 145
^{1}H NMR (500MHz, THF-d$_8$) δ: 7.48 (d, *J*=8.85 Hz, 4 H); 6.96 (d, *J*=8.85 Hz, 4 H); 6.76 (m, 4 H); 4.03 (t, *J*=6.41 Hz, 4 H); 1.82 (m, 4 H); 1.46 (m, 8 H); 0.98 (t, *J*=7.17 Hz, 6 H)
^{13}C NMR (125 MHz, THF-d$_8$) δ: 160.94; 147.18; 138.02; 133.66; 117.35; 115.48; 114.70; 108.06; 95.37; 78.65; 68.73; 29.82; 29.13; 23.31; 14.35;

5,5'-bis{[4-(pentylthio)phenyl]ethynyl}-2,2'-bifuran (PEF-5S)

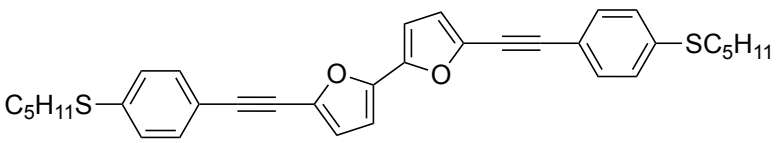

Yield: 47%
Purity 98.5% (HPLC-PDA)
MS(EI) m/z: 538; 467; 397; 366; 335; 306; 276; 250; 207; 170; 139

^{1}H NMR (500MHz, THF-d_8) δ: 7.46 (d, *J*=8.55 Hz, 4 H); 7.34 (d, *J*=8.55 Hz, 4 H); 6.84 (d, *J*=3.66 Hz, 2 H); 6.79 (d, *J*=3.66 Hz, 2 H); 3.03 (t, *J*=7.32 Hz, 4 H); 1.71 (m, 4 H); 1.43 (m, 8 H); 0.94 (t, *J*=7.17 Hz, 6 H)
^{13}C NMR (125 MHz, THF-d_8) δ: 147.36; 140.69; 137.73; 132.31; 128.11; 119.31; 118.02; 108.35; 95.19; 80.11; 32.85; 31.90; 29.54; 23.10; 14.29

5,5'-bis[(4-pentylphenyl)ethynyl]-2,2'-bithiophene (PET-5)

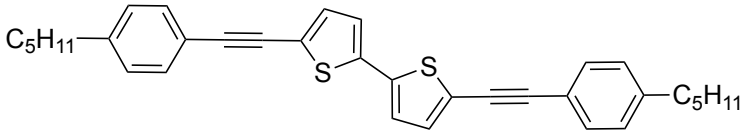

Yield:72%
Purity 99.1% (HPLC-PDA)
MS(EI) m/z: 506; 463; 449; 392; 358; 312; 253; 225; 196
^{1}H NMR (500MHz, THF-d_8) δ: 7.45 (d, *J*=7.93 Hz, 4 H); 7.24 (m, 8 H); 2.66 (t, *J*=7.63 Hz, 4 H); 1.66 (m, 4 H); 1.37 (m, 8 H); 0.94 (t, *J*=6.87 Hz, 6 H)
^{13}C NMR (125 MHz, THF-d_8) δ: 144.74; 138.60; 133.65; 132.06; 129.37; 125.09; 123.65; 120.85; 95.56; 82.33; 36.60; 32.38; 31.82; 23.37; 14.33

5,5'-bis{[4-(pentyloxy)phenyl]ethynyl}-2,2'-bithiophene (PET-5O)

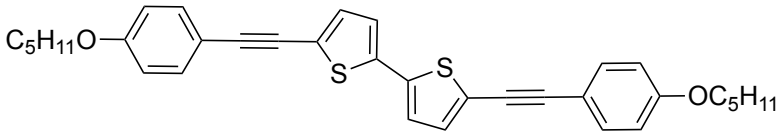

Yield: 66%
Purity 99,5% (HPLC-PDA)
MS(EI) m/z: 538; 468; 398; 380; 369; 335; 306; 199; 161
^{1}H NMR (500MHz, THF-d_8) δ: 7.45 (d, *J*=8.85 Hz, 4 H); 7.20 (m, 4 H); 6.95 (d, *J*=8.85 Hz, 4 H); 4.02 (t, *J*=6.56 Hz, 4 H); 1.82 (m, 4 H); 1.47 (m, 8 H); 0.98 (t, *J*=7.17 Hz, 6 H)
^{13}C NMR (125 MHz, THF-d_8) δ: 160.75; 138.32; 133.59; 133.25; 124.94; 123.90; 115.40; 115.30; 95.57; 81.47; 68.70; 29.83; 29.13; 23.32; 14.35

5,5'-bis{[4-(pentylthio)phenyl}ethynyl]-2,2'-bithiophene (PET-5S)

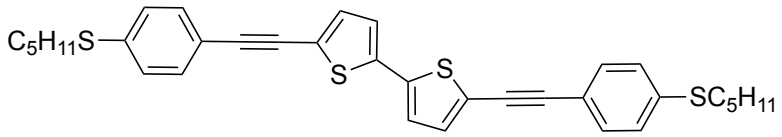

Yield: 70%
Purity 98,2% (HPLC-PDA)
MS(EI) m/z: 570; 499; 468; 429; 385; 364; 332; 285; 250; 227; 215; 195; 145
^{1}H NMR (500MHz, THF-d_8) δ: 7.44 (d, *J*=8.55 Hz, 4 H); 7.32 (d, *J*=8.55 Hz, 4 H); 7.24 (m, 4 H); 3.02 (t, *J*=7.63 Hz, 4 H); 1.70 (m, 4 H); 1.42 (m, 8 H); 0.94 (t, *J*=7.17 Hz, 6 H)
^{13}C NMR (125 MHz, THF-d_8) δ: 140.31; 138.71; 133.80; 132.33; 128.20; 125.17; 123.51; 119.99; 95.27; 83.05; 32.96; 31.89; 29.55; 23.10; 14.27

5,5'-Bis[(4-pentylphenyl)ethynyl]-2,2'-biselenophene (PES-5)

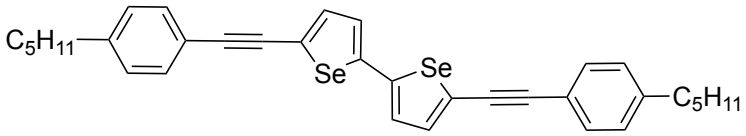

Yield: 65%.
Purity 98.5% (HPLC-PDA)
MS(EI) m/z: 601.75; 544.70; 487.70; 407.80; 325.90; 243.80; 188.95; 139.00; 115.05
^{1}H NMR (500MHz, THF-d_8) δ: 7.43 (d, *J*=7.93 Hz, 4 H); 7.36 (d, *J*=3.97 Hz, 2 H); 7.30 (d, *J*=3.97 Hz, 2 H); 7.23 (d, *J*=8.24 Hz, 4 H); 2.65 (t, *J*=7.63 Hz, 4 H); 1.66 (m, 4 H); 1.38 (m, 8 H); 0.93 (t, *J*=6.87 Hz, 6 H)
^{13}C NMR (125 MHz, THF-d_8) δ: 145.48; 143.76; 134.94; 131.03; 128.44; 127.11; 126.82; 120.15; 96.54; 83.80; 35.68; 31.45; 30.89; 22.45; 13.40

5,5'-Bis{[4-(pentyloxy)phenyl}ethynyl]-2,2'-biselenophene (PES-5O)

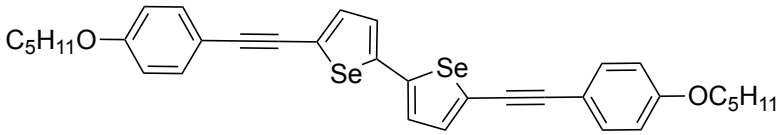

Yield: 56%.
Purity 98.5% (HPLC-PDA)
MS(EI) m/z: 631.75; 560.70; 491.65; 462.65; 413.80; 333.95; 276.00; 208.80; 163.00; 113.00
^{1}H NMR (500MHz, nitrobenzene-d_5/DMSO-d_6) δ: 7.44 (d, J=8.85 Hz, 4 H); 7.31 (m, 2 H); 7.19 (d, J=3.97 Hz, 2 H); 6.90 (d, J=8.85 Hz, 3 H); 3.94 (t, J=6.56 Hz, 4 H); 1.70 (m, 4 H); 1.33 (m, 8 H); 0.84 (t, J=7.17 Hz, 6 H)

5,5'-Bis{[4-(pentylthio)phenyl}ethynyl]-2,2'-biselenophene (PES-5S)

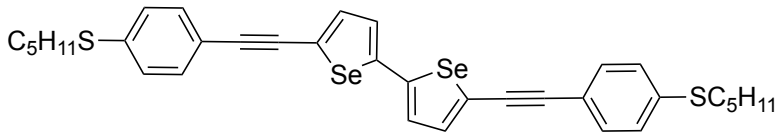

Yield: 52%.
Purity 99.7% (HPLC-PDA)
MS(EI) m/z: 665.80; 593.00 (poor ionization observed)
^{1}H NMR (500MHz, nitrobenzene-d_5/DMSO-d_6) δ: 7.38 (d, J=8.24 Hz, 2 H); 7.31 (d, J=3.97 Hz, 1 H); 7.26 (d, J=8.55 Hz, 2 H); 7.15 (d, J=3.36 Hz, 1 H); 2.89 (t, J=7.32 Hz, 2 H); 1.61 (m, 2 H); 1.33 (m, 4H), 0.85 (t, J=7.32 Hz, 3 H)

Mesomorphic properties

Phase sequence of final compounds was determined with the polarization optical microscopy (POM) and thermodynamical data was measured with DSC. Table below summarizes mesomorphic properties of synthesized compounds.

Table S1. Mesomorphic properties of compounds – phase sequence, phase transition temperatures and enthalpies of transitions.

	Cr	T[°C] (dH[kJ/mol])	Cr II	T[°C] (dH[kJ/mol])	Cr III	T[°C] (dH[kJ/mol])	SmA	T[°C]	N	T[°C] (dH[kJ/mol])	Iso
PEF-5	*	129.8 (-36.49)									*
PEF-5O	*	150.0 (-47.10)							(*)	(149)[a]	*
PEF-5S	*	153.3 (-46.09)									*
PET-5	*	132.0 (-31.82)							*	212.2 (-1.13)	*
PET-5O	*	168.3 (-36.17)							*	233.5 (-1.46)	*
PET-5S	*	152.7 (-32.07)							*	167.9 (-0.63)	*
PES-5	*	160.0 (-16.22)	*	179.6 (-1.25)	*	192.9 (-14.60)			*	254[a]	*
PES-5O	*	202.6 (-2.96)	*	205.1 (-38.05)					*	234[a]	*
PES-5S	*	165.2 (-16.91)	*	206.1 (-11.69)			*	219[a]	*	228[a]	*

[a] phase transition was observed only with POM

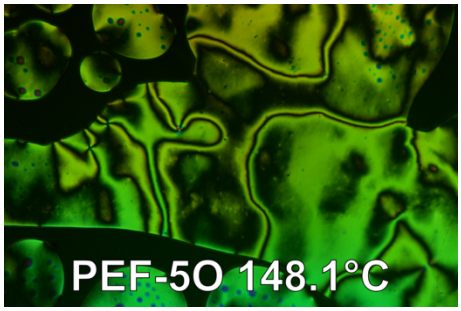

Figure S1. POM image of PEF-5O.

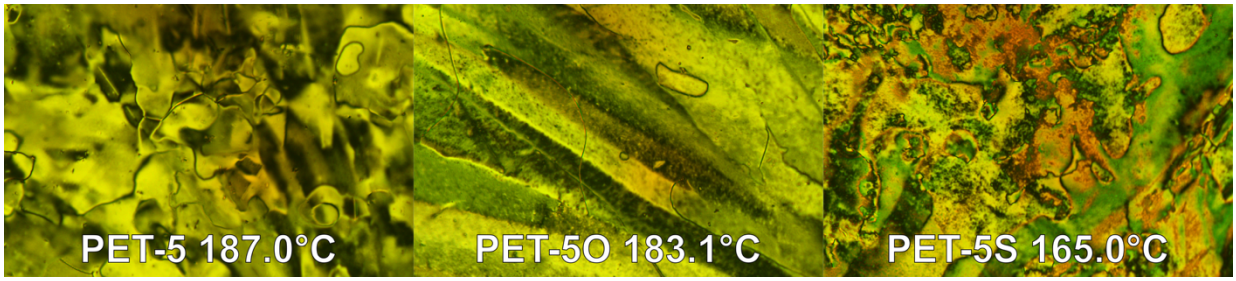

Figure S2. POM images of PET-5, PET-5O, and PET-5S.

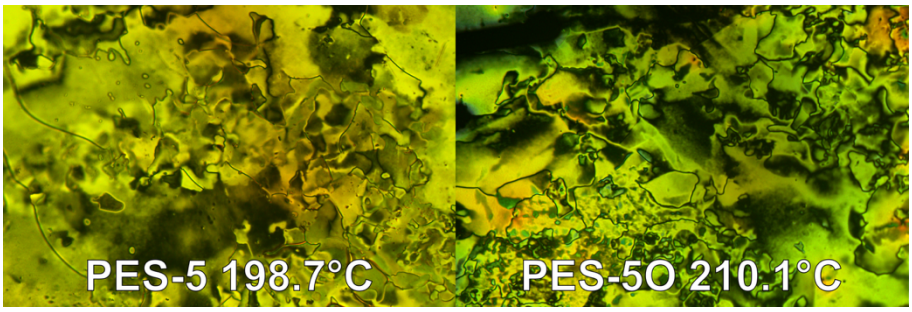

Figure S3. POM images of PES-5 and PES-5O.

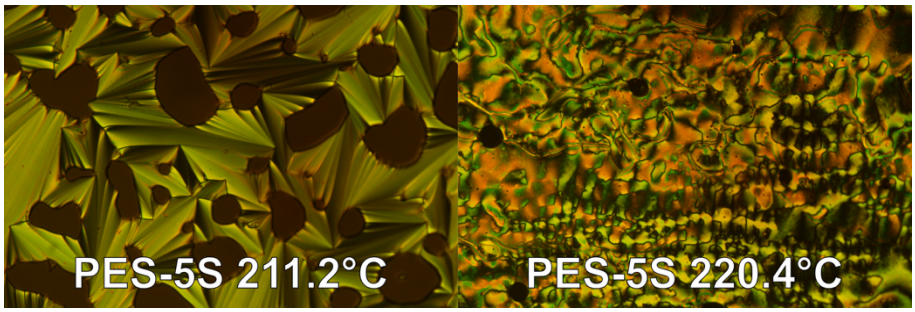

Figure S4. POM images of PES-5S.

Spectral properties

Table S2. TD-DFT calculated vertical energies of the lowest singlet (S_1) and triplet (T_1, T_2) excited states and the corresponding singlet–triplet energy gaps ($\Delta E(S_1–T_1)$, $\Delta E(S_1–T_2)$). All values in eV.

Compound	S_1	T_1	$\Delta E(S_1-T_1)$	T_2	$\Delta E(S_1-T_2)$
PEF-5	3.06	2.08	0.98	2.71	0.35
PEF-5O	3.05	2.08	0.97	2.71	0.34
PEF-5S	2.98	2.05	0.93	2.62	0.36
PET-5	2.86	1.91	0.95	2.64	0.22
PET-5O	2.85	1.92	0.93	2.62	0.23
PET-5S	2.80	1.90	0.91	2.55	0.25
PES-5	2.74	1.78	0.96	2.57	0.17
PES-5O	2.71	1.77	0.94	2.56	0.15
PES-5S	2.68	1.77	0.91	2.50	0.18

Table S3. Chromaticity coordinates of bifuran compounds compared to the industry standard (Rec. 709).

Compound	x,y coordinates of PEF-series compounds	Rec.709 (BT. 709) x,y coordinates	Similarity of the compounds' chromaticity coordinates (x, y) to the (x, y) coordinates of the Rec. 709 standard
PEF-5	(0.15628, 0.05661	(0.1500, 0.0600)	(95.81%, 94.35%)
PEF-5O	(0.15449, 0.06469)		(97.01%, 92.18%)
PEF-5S	(0.15246, 0.08442)		(98.36%, 59.3%)

As seen in Figure 7a (main text), absorption for bifuran derivatives spans from approximately 300 to about 430 nm. Additionally, for the PEF-5O derivative, a long-wavelength absorption tail extending to about 500 nm is noted. The absorbance maxima are located at 360 nm for the PEF-5 and PEF-5O. For PEF-5S, the highest peak is observed at around 370 nm, with an additional emerging one at 315 nm. In the case of the second group of bithiophene derivatives (Figure 7b), PET-5, PET-5O, and PET-5S exhibit an absorption range extending from about 300 to over 600 nm. The maximum for PET-5 is located at 385 nm. For PET-5O it is noticeable at 325 nm with a second emerging one, visible at 385 nm. Measurement of PET-5S shows maxima at wavelengths of 325 nm and 400 nm (the less intense peak). The last group of compounds, namely biselenophenes, demonstrates an absorption range (Figure 7c) spanning from 300 to about 500 nm (PES-5), and 300-500 nm with an absorption tail extending up to 800 nm (PES-5O and PES-5S). In this case, for PES-5, a maximum is noted at 350 nm, and a less intense one is located at 410 nm. PES-5O exhibits two maxima placed at 355 nm and 406 nm. A similar situation is observed for PES-5S.

Theoretical calculations

Among synthesized compounds containing alkyl or thioalkyl chain, the predominant conformers are those where the side chains are oriented either parallel or antiparallel to the flat molecular backbone, corresponding to the C_2 or C_i symmetry point groups, respectively (Figure S1). The abundance of both conformers in the global population is nearly equal. In contrast, for compounds containing pentyloxy terminal group, the dominant conformer features alkyl chains lying in the plane of the main skeleton. This conformer, belonging to the C_2 symmetry point group, constitutes approximately 90% of the total population (Table S2).

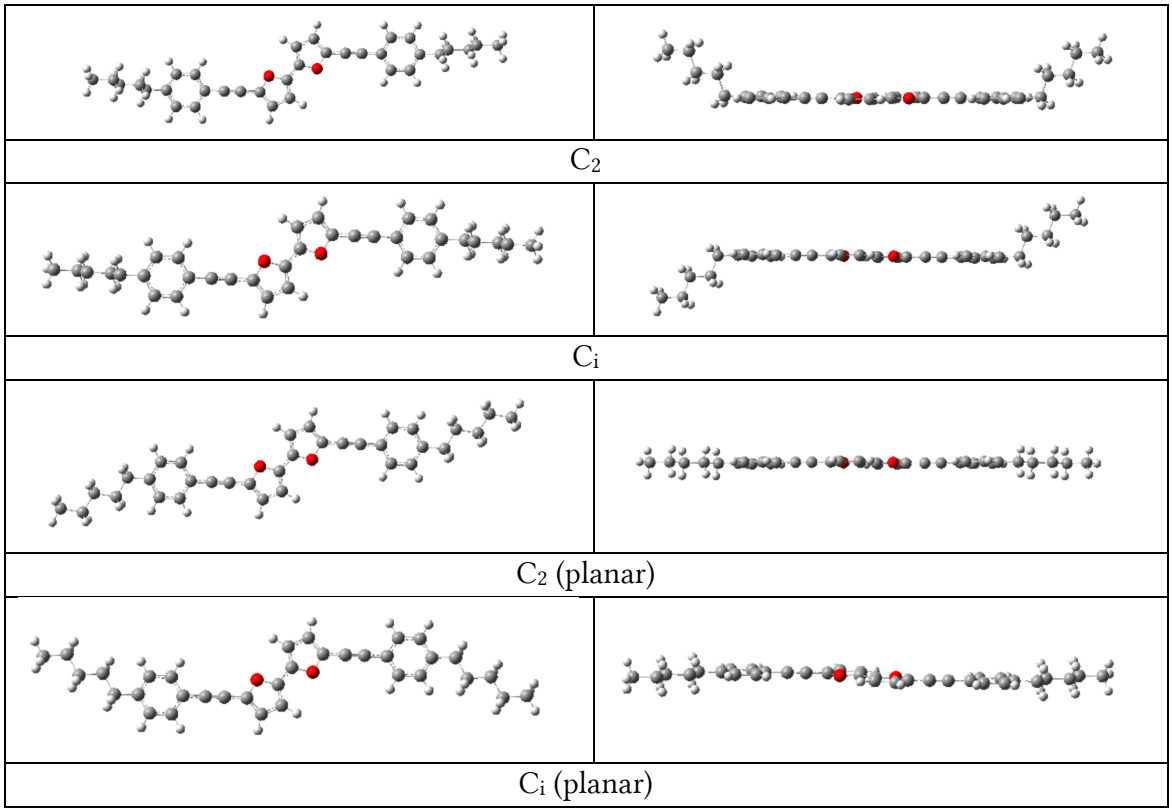

Figure S5. Structures of conformer with different symmetry in two projections.

Table S4. Energy differences between Chalcogenophene Triad conformers (kcal/mol) in the ground state. The percentage of conformers in the total population is given in parentheses.

		C_2	C_i	C_2 (planar)
PEF-5		**0.00 (48)**	0.004 (47)	1.75 (3)
PEF-5O		1.53 (7)	1.54 (6)	**0.00 (87)**
PEF-5S		**0.00 (45)**	0.02 (44)	0.08 (11)
PET-5		**0.00 (48)**	0.02 (47)	1.76 (3)
PET-5O		1.53 (7)	1.54 (6)	**0.00 (87)**
PET-5S		**0.00 (45)**	0.02 (44)	0.08 (11)
PES-5		**0.00 (48)**	0.003 (47)	1.66 (3)
PES-5O		1.53 (6)	1.54 (5)	**0.00 (89)**
PES-5S		**0.00 (45)**	0.02 (42)	0.75 (13)

Table S5. Geometric descriptors from calculated structures.

	Ring opening angle [°]	Bend angle [°]	Core aspect ratio	Heterocycle coplanarity angle [°]	Lateral deviation [Å]
PEF-5	133.45	179.44	4.40	0.40	1.11
PEF-5O	134.42	179.59	4.39	0.40	1.11
PEF-5S	134.46	179.66	4.41	0.15	1.10
PEF average	**134.44 ± 0.02**	**179.5 ± 0.11**	**4.40±0.01**	**0.31 ± 0.14**	**1.11 ± 0.00**
PET-5	152.40	177.27	5.59	8.52	0.74
PET-5O	152.37	175.82	5.60	11.63	0.74
PET-5S	152.36	177.24	5.57	9.83	0.75
PET average	**152.38 ± 0.02**	**176.78 ± 0.83**	**5.59±0.01**	**9.99 ±1.56**	**0.74 ± 0.00**
PES-5	156.78	179.69	5.96	1.31	0.64
PES-5O	156.82	179.69	5.98	0.91	0.64
PES-5S	156.83	179.75	5.99	3.96	0.64
PES average	**156.81 ± 0.03**	**179.71 ± 0.04**	**5.98 ±0.02**	**2.06 ± 1.66**	**0.64 ± 0.00**

The **ring opening angle** is the angle defined by the 2,5-positions of the heterocycle and reflects its intrinsic local curvature. The **bend angle** describes the overall linearity of the rigid core, with values closer to 180° corresponding to a more linear structure. The **core aspect ratio** expresses the elongation of the rigid core and serves as a measure of effective molecular anisometry. The **heterocycle coplanarity angle** represents the dihedral mismatch between the two heterocyclic rings, with lower values indicating a more coplanar arrangement. The **lateral deviation** denotes the average absolute displacement of the heterocyclic rings from the terminal-ring axis and reflects the extent of zig-zag distortion within the molecular core.

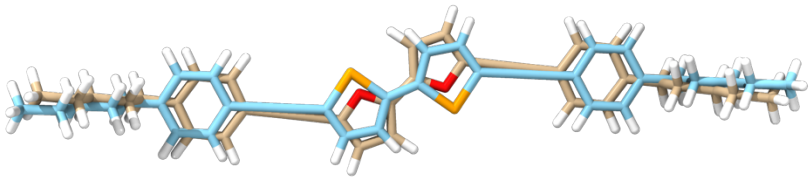

Figure S6. Superimposed optimized geometries of PEF-5 (beige) and PES-5 (blue).

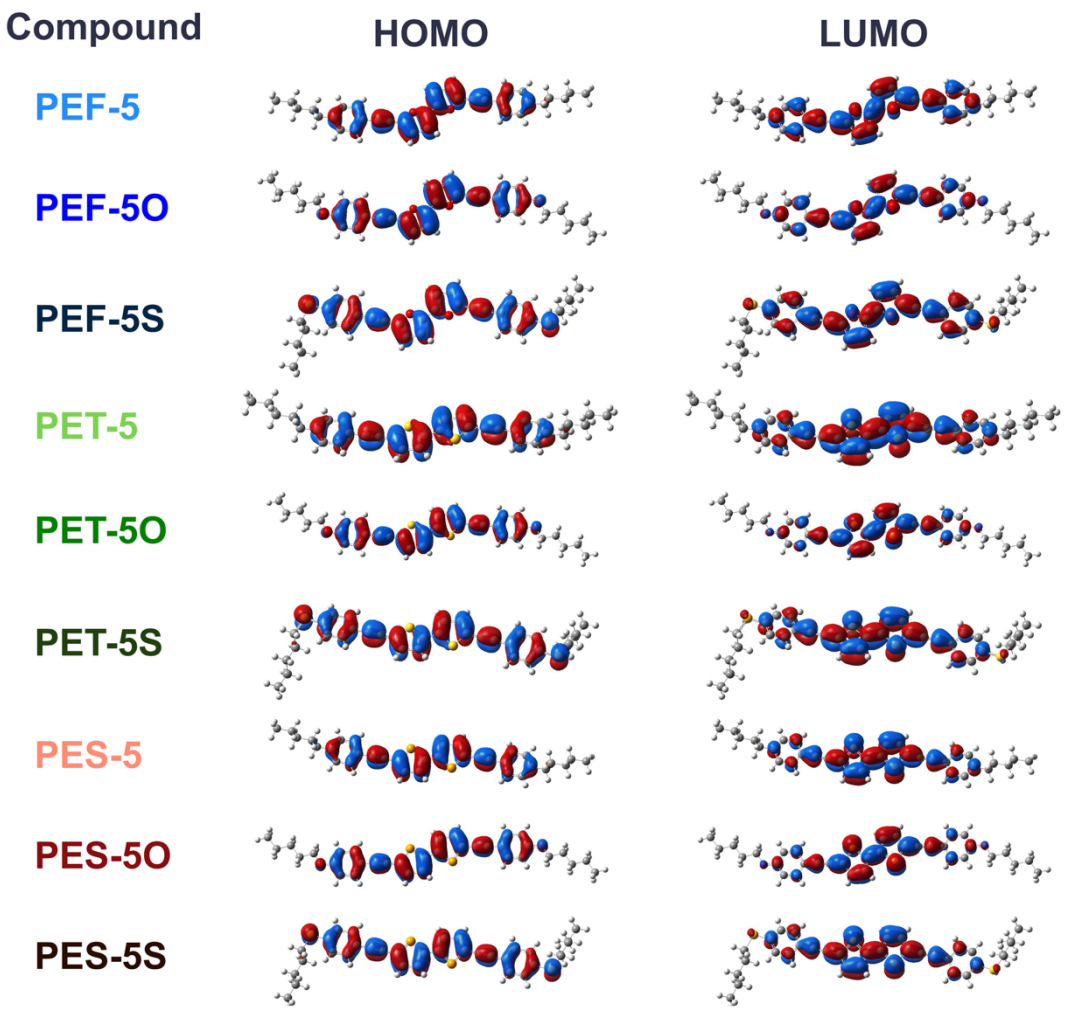

Figure S7. Frontier orbitals involved in one-photon $S_0 \rightarrow S_1$ transition.

Table S6. Dihedral angles (deg) and CC inter-ring distances (A) of the studied compounds in the ground (S_0) and excited (S_1) states.

	S_0			S_1		Δ	
	θ_0(XCCX)	r_0(CC)		θ_1(XCCX)	r_1(CC)	θ	r
PEF-5	179.6	1.440	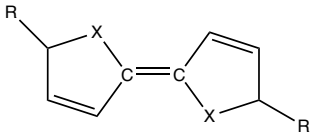	179.9	1.386	0.3	0.054
PEF-5O	179.6	1.440		180.0	1.387	0.4	0.053
PEF-5S	179.9	1.440		179.9	1.388	0.0	0.052
PET-5	171.5	1.452		179.9	1.391	8.4	0.061
PET-5O	168.3	1.452		180.0	1.391	11.7	0.061
PET-5S	170.3	1.452		179.9	1.393	9.6	0.059
PES-5	178.8	1.446		179.9	1.385	1.1	0.061
PES-5O	179.2	1.446		180.0	1.386	0.8	0.060
PES-5S	176.7	1.446		180.0	1.387	3.3	0.059

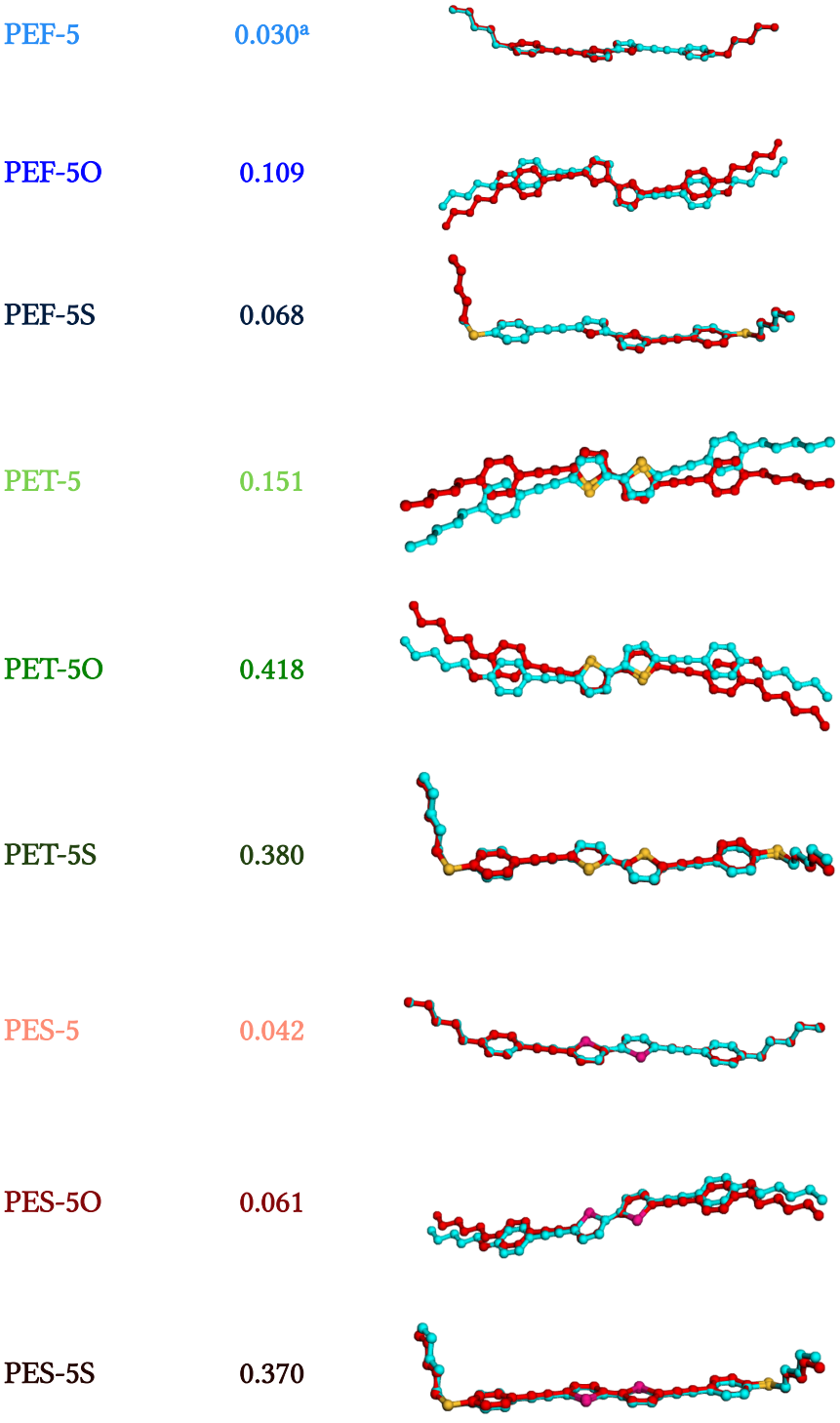

Figure S8. Molecular structures of ground (S_0, blue) and excited state (S_1, red), [a]RMSD values in Å.

DSC thermograms

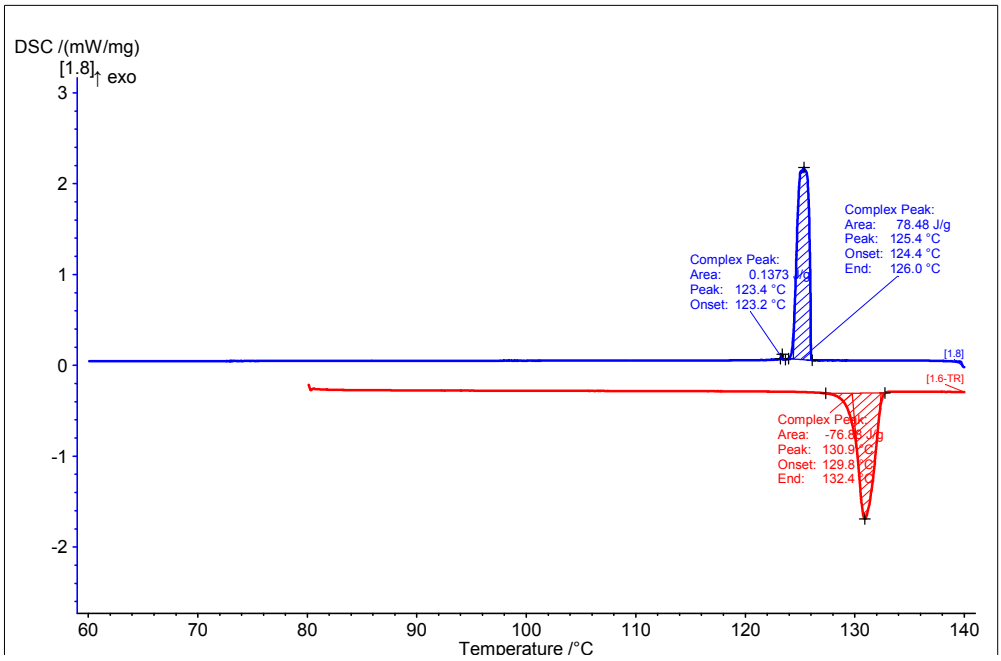

Figure S9. PEF-5

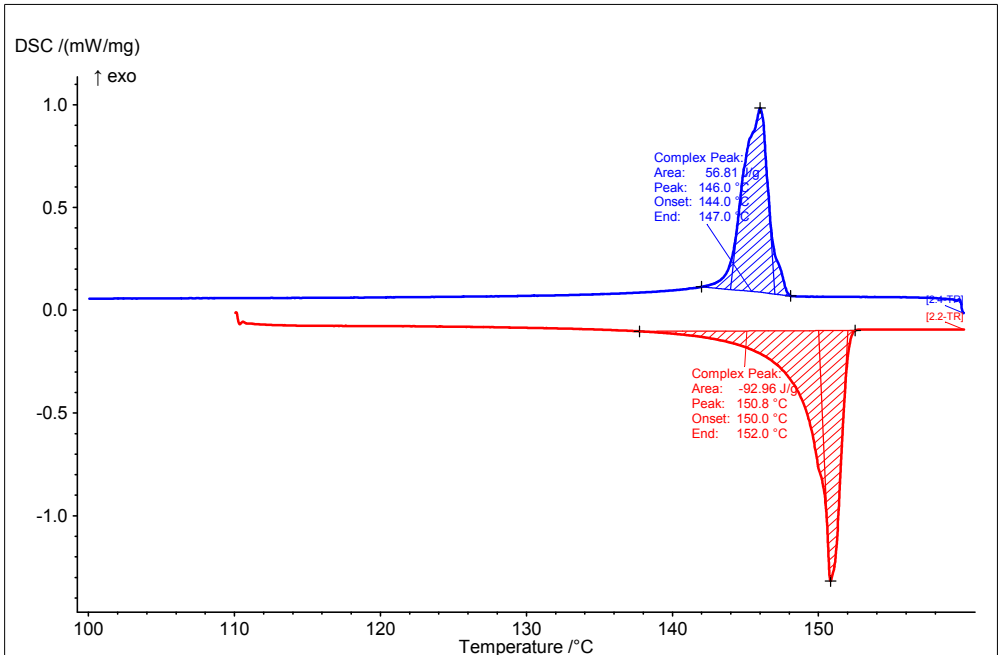

Figure S10. PEF-5O

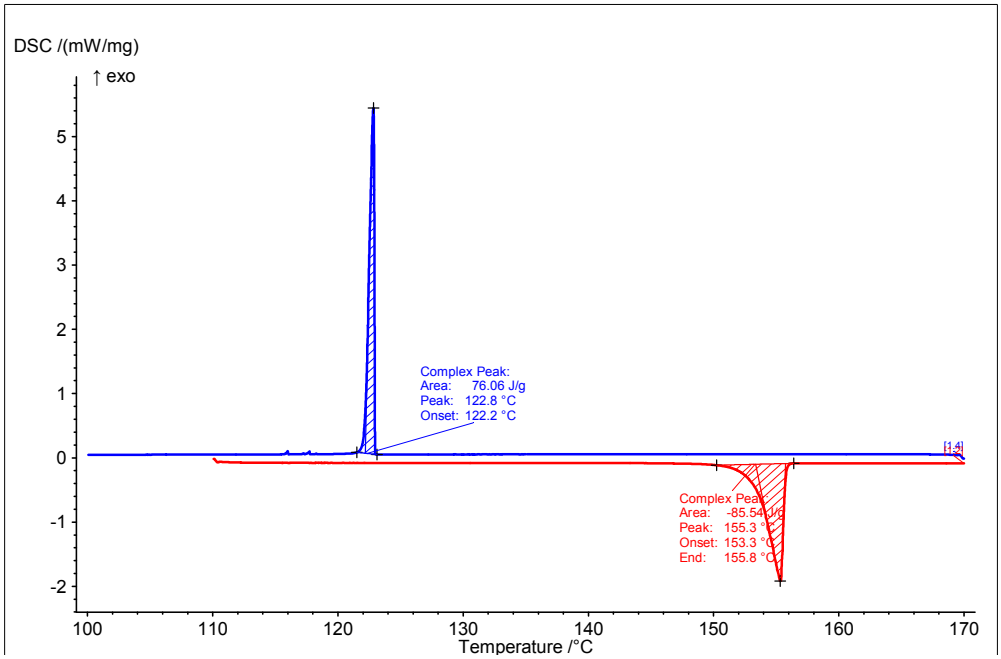

Figure S11. PEF-5S

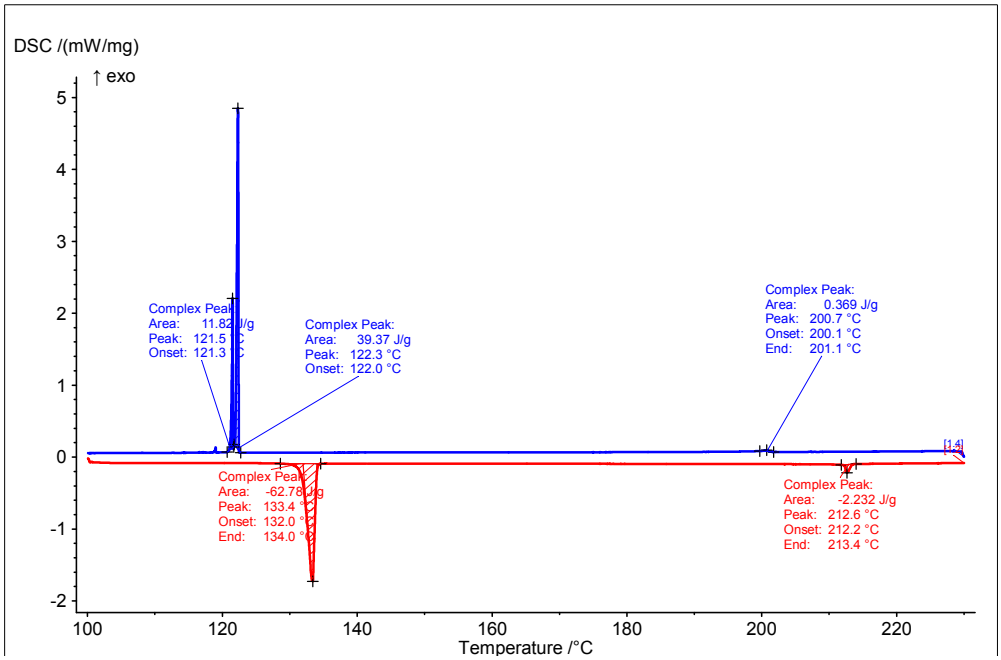

Figure S12. PET-5

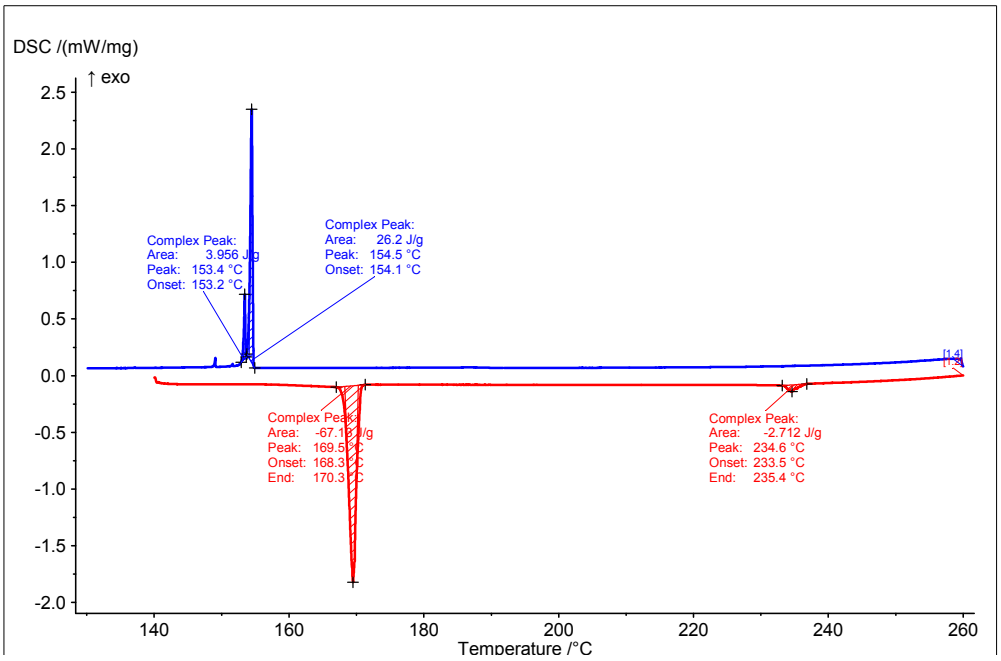

Figure S13. PET-5O

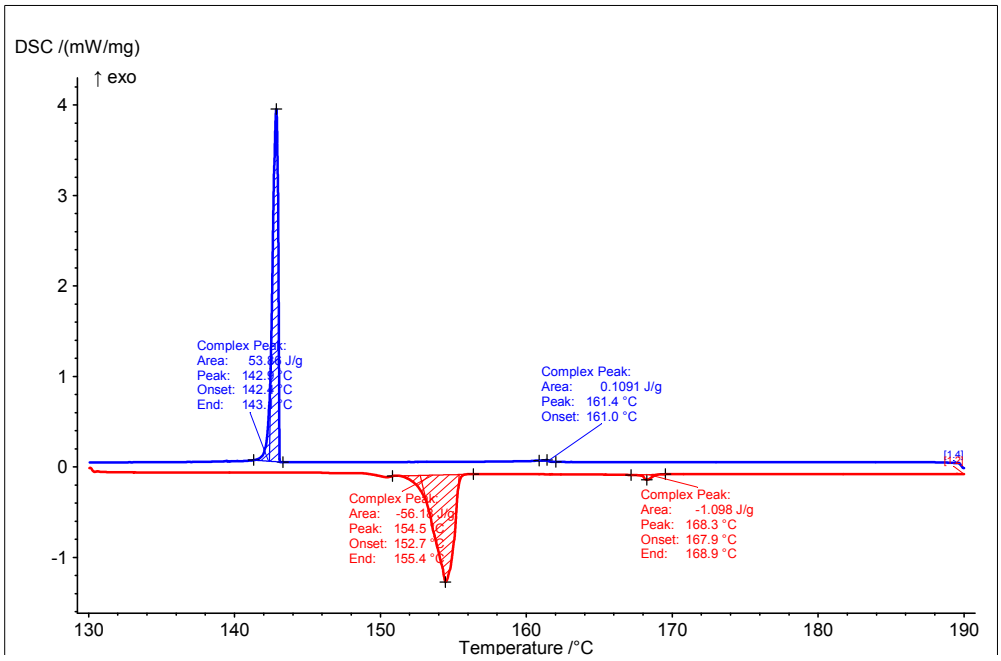

Figure S14. PET-5S

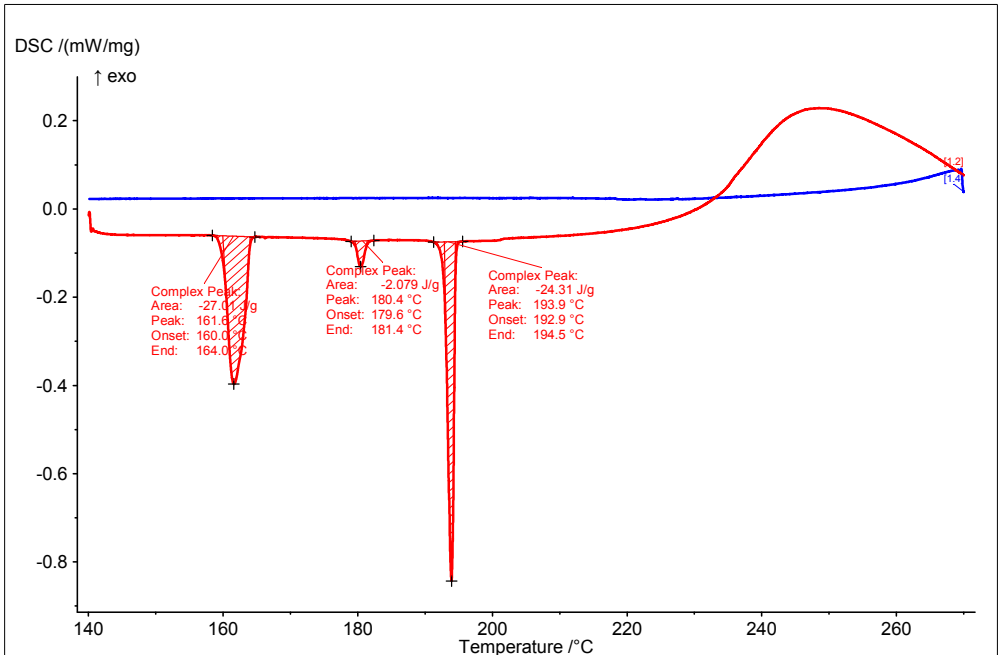

Figure S15. PES-5

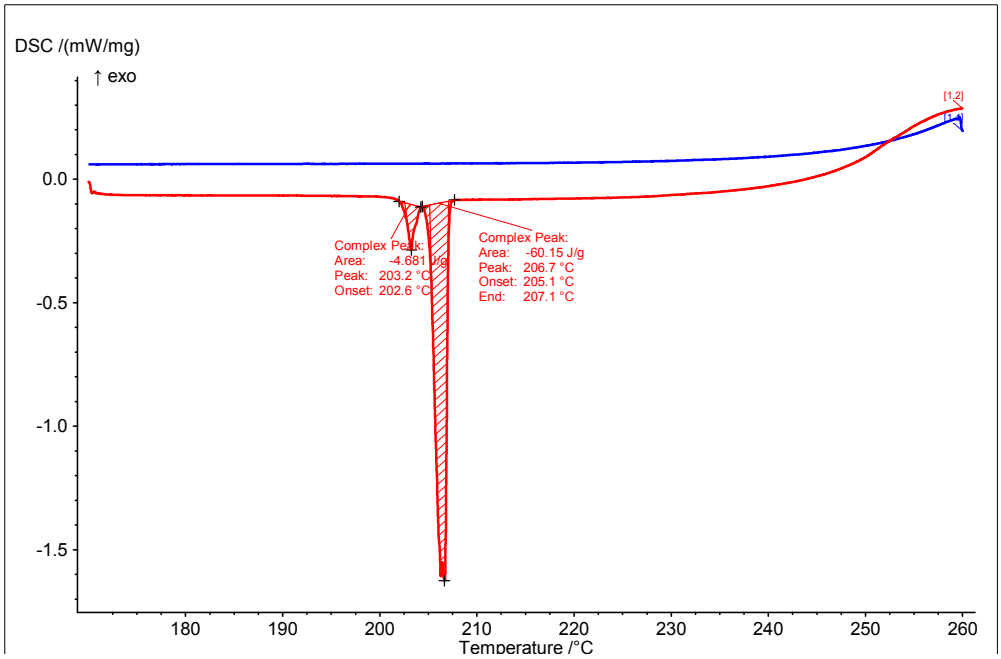

Figure S16. PES-5O

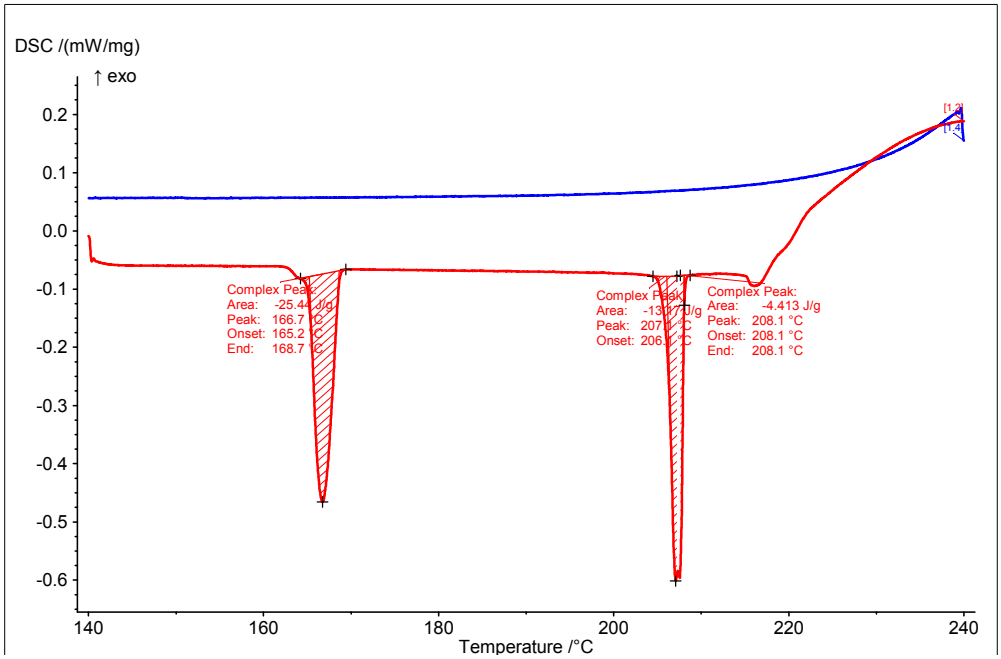

Figure S17. PES-5S

NMR spectra

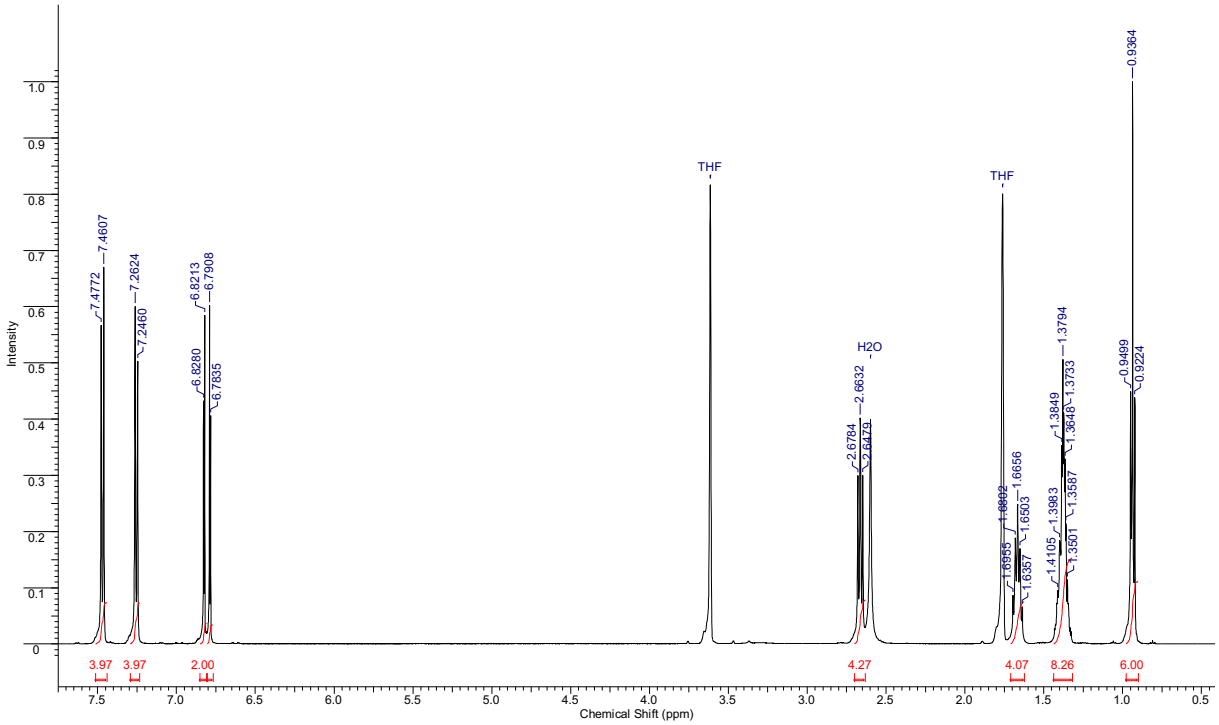

Figure S18. ^{1}H NMR spectrum of PEF-5 (500MHz, THF-d_8).

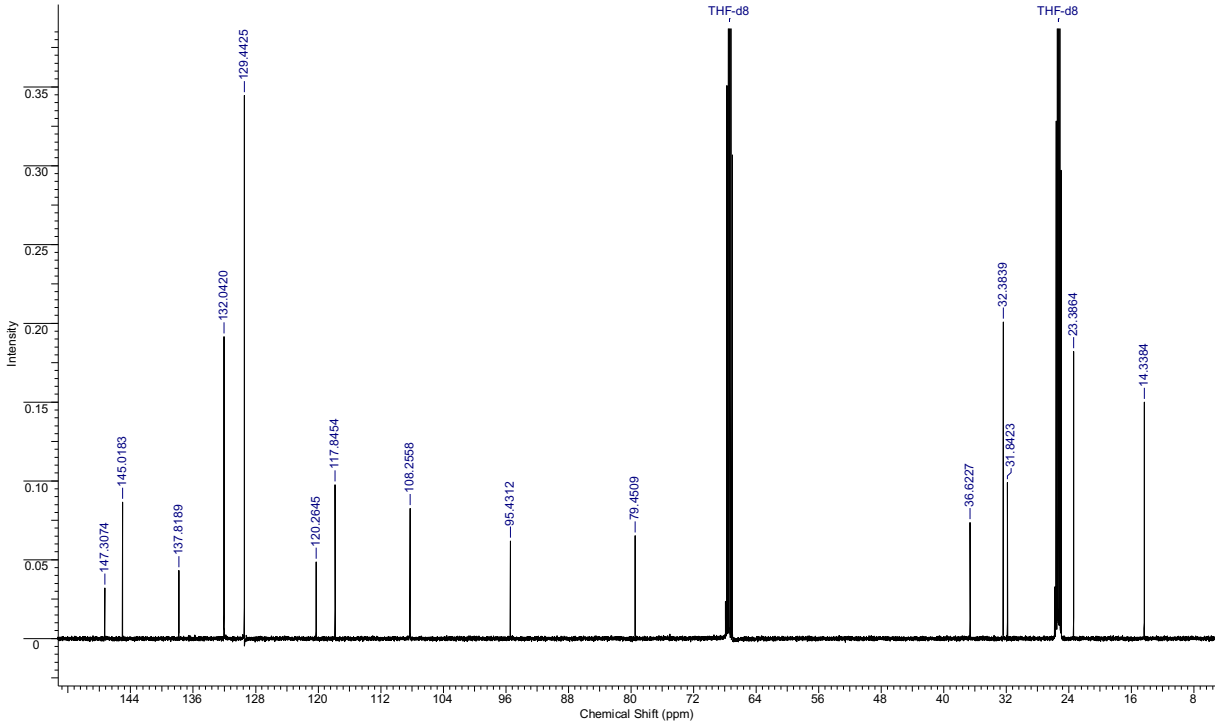

Figure S19. ^{13}C NMR spectrum of PEF-5 (125 MHz, THF-d_8).

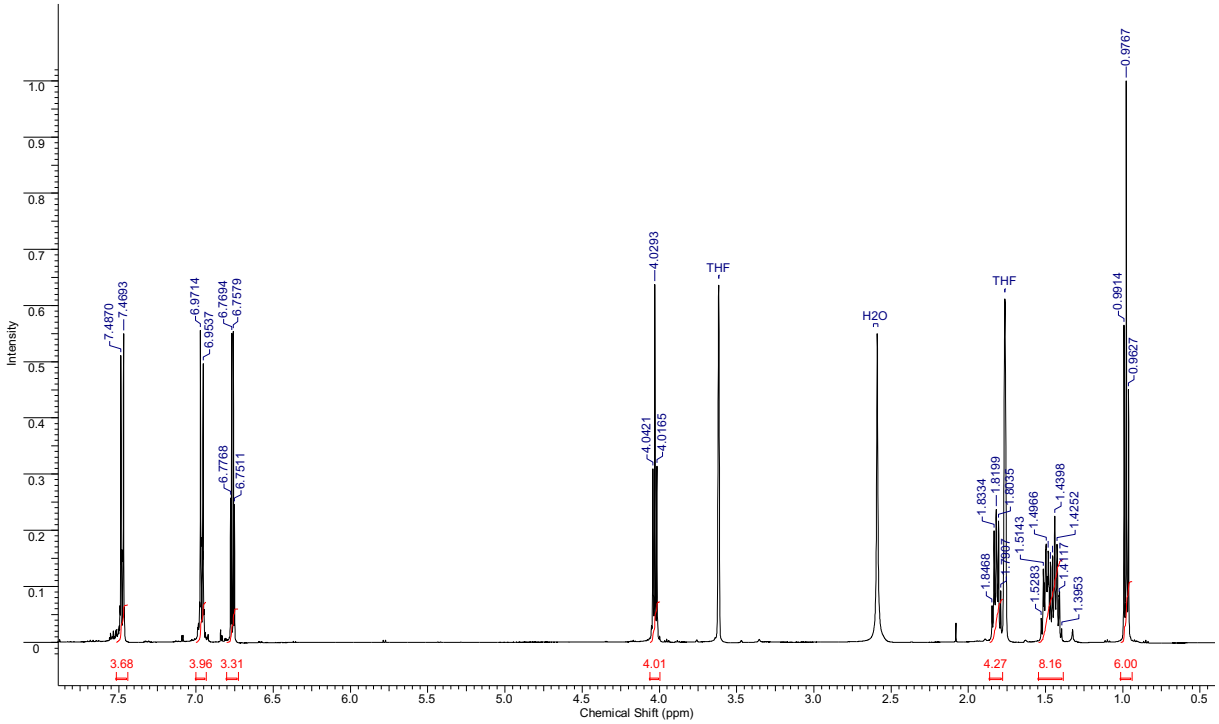

Figure S20. ^{1}H NMR spectrum of PEF-5O (500MHz, THF-d_8).

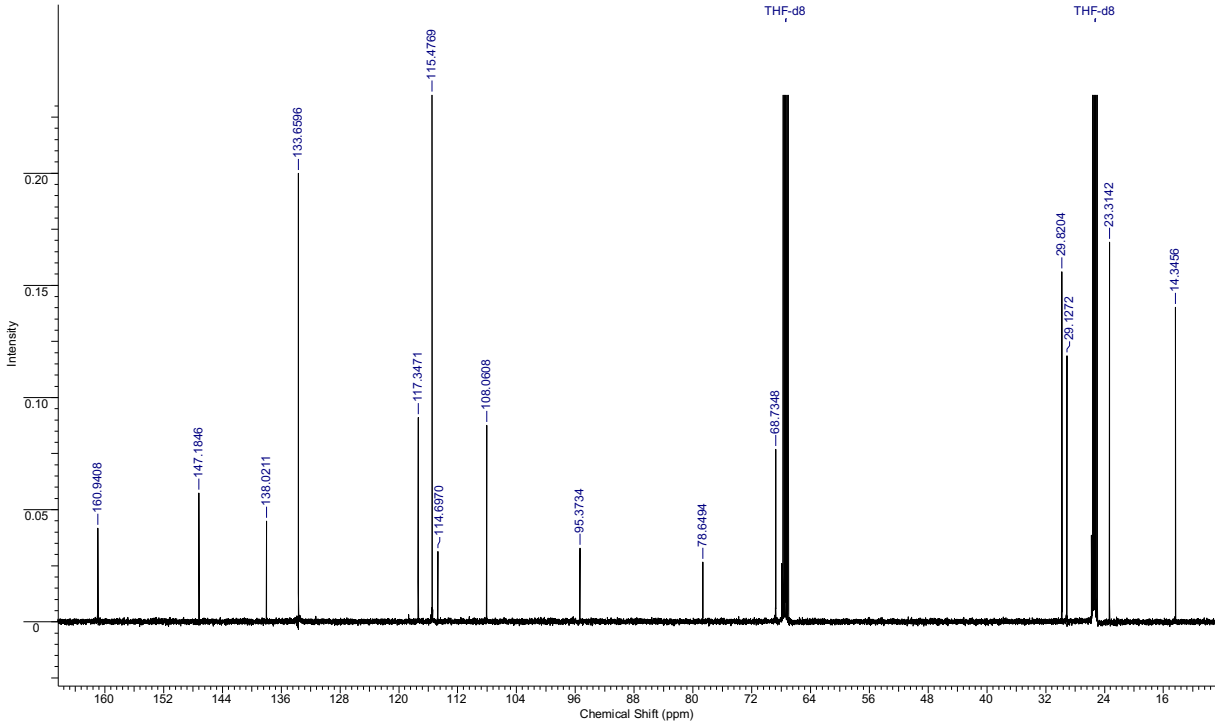

Figure S21. ^{13}C NMR spectrum of PEF-5O (125 MHz, THF-d_8).

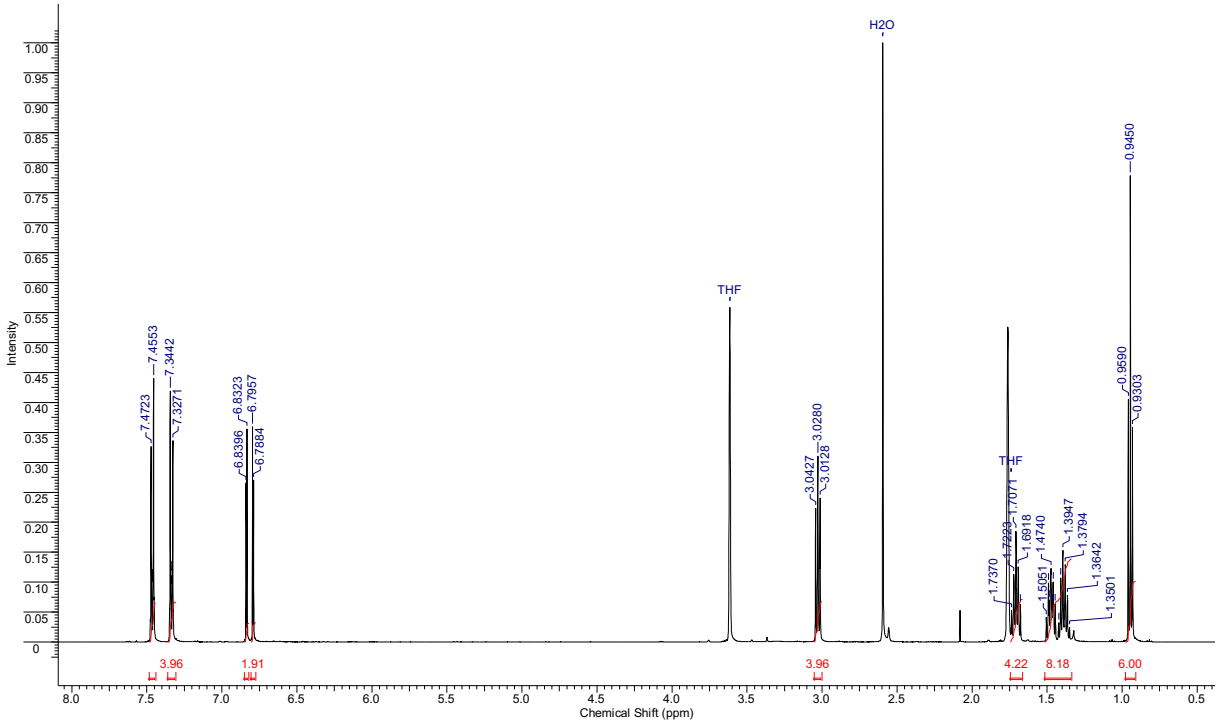

Figure S22. ^{1}H NMR spectrum of PEF-5S (500MHz, THF-d_8).

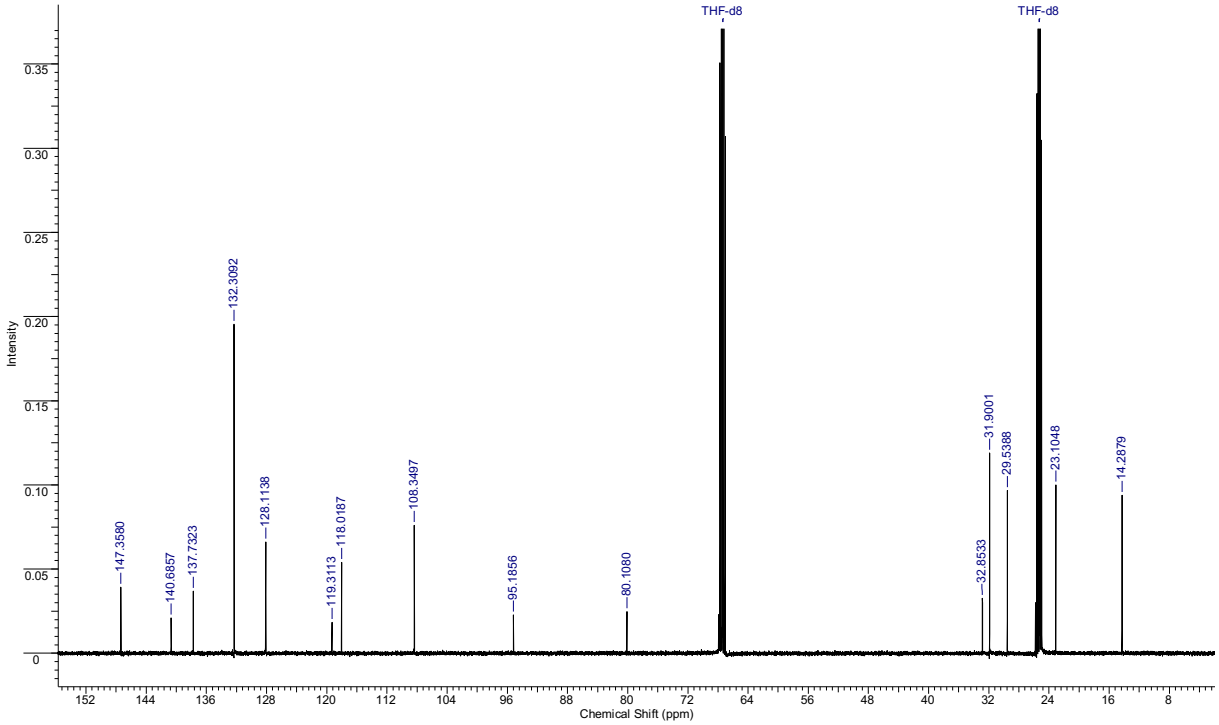

Figure S23. ^{13}C NMR spectrum of PEF-5S (125 MHz, THF-d_8).

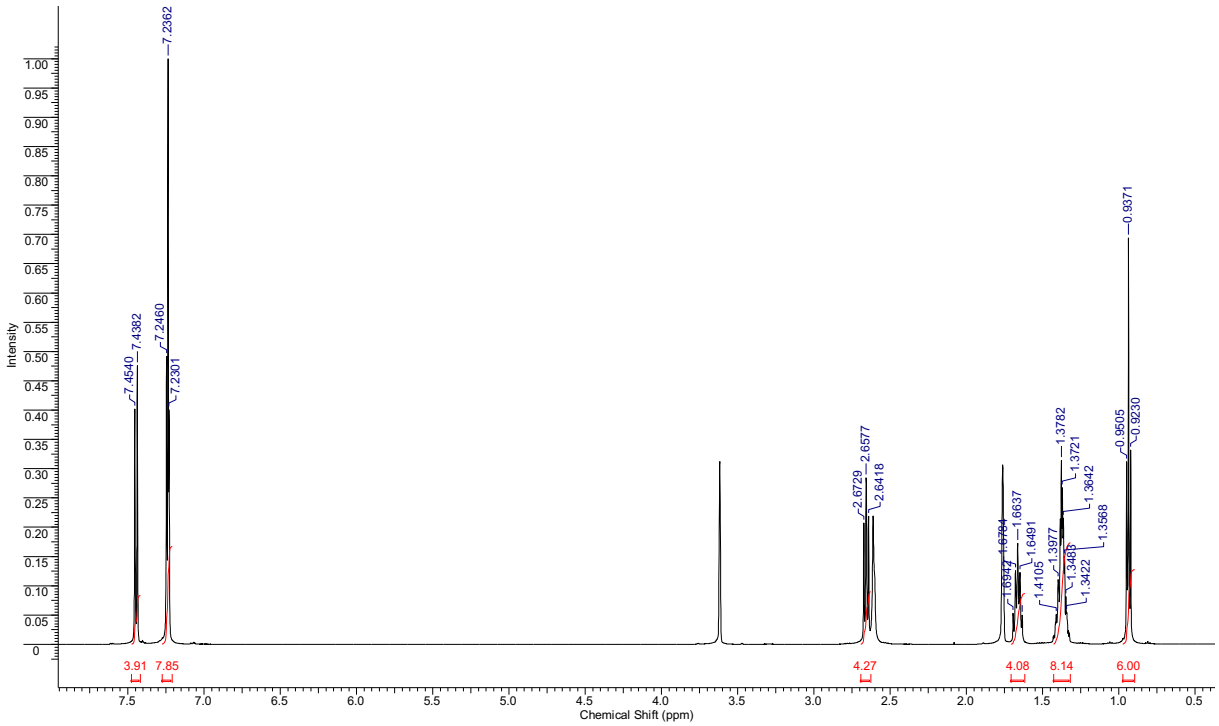

Figure S24. ^{1}H NMR spectrum of PET-5 (500MHz, THF-d_8).

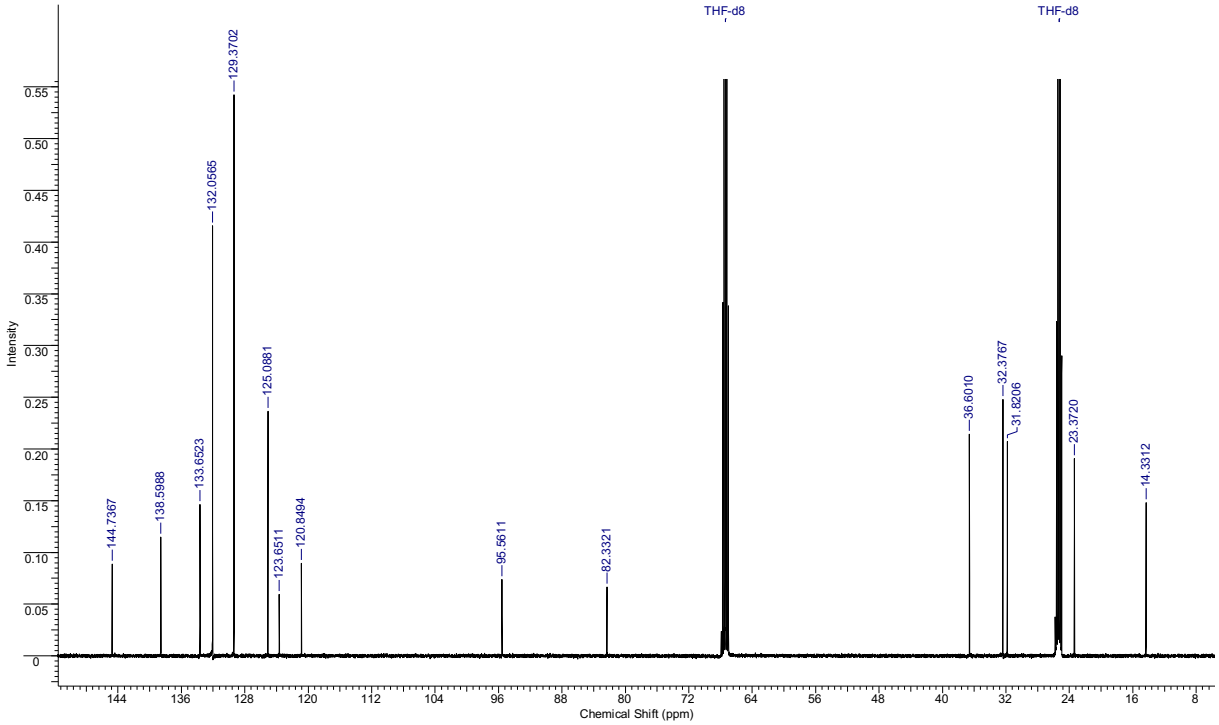

Figure S25. ^{13}C NMR spectrum of PET-5 (125 MHz, THF-d_8).

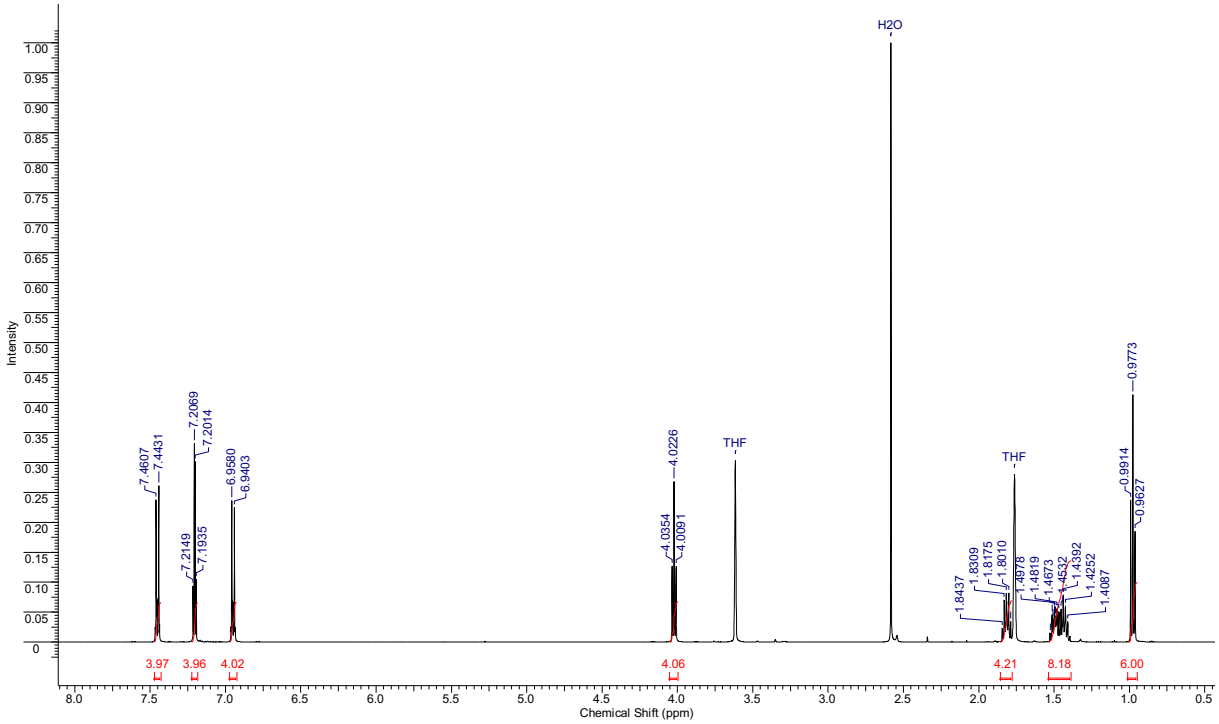

Figure S26. ^{1}H NMR spectrum of PET-5O (500MHz, THF-d_8).

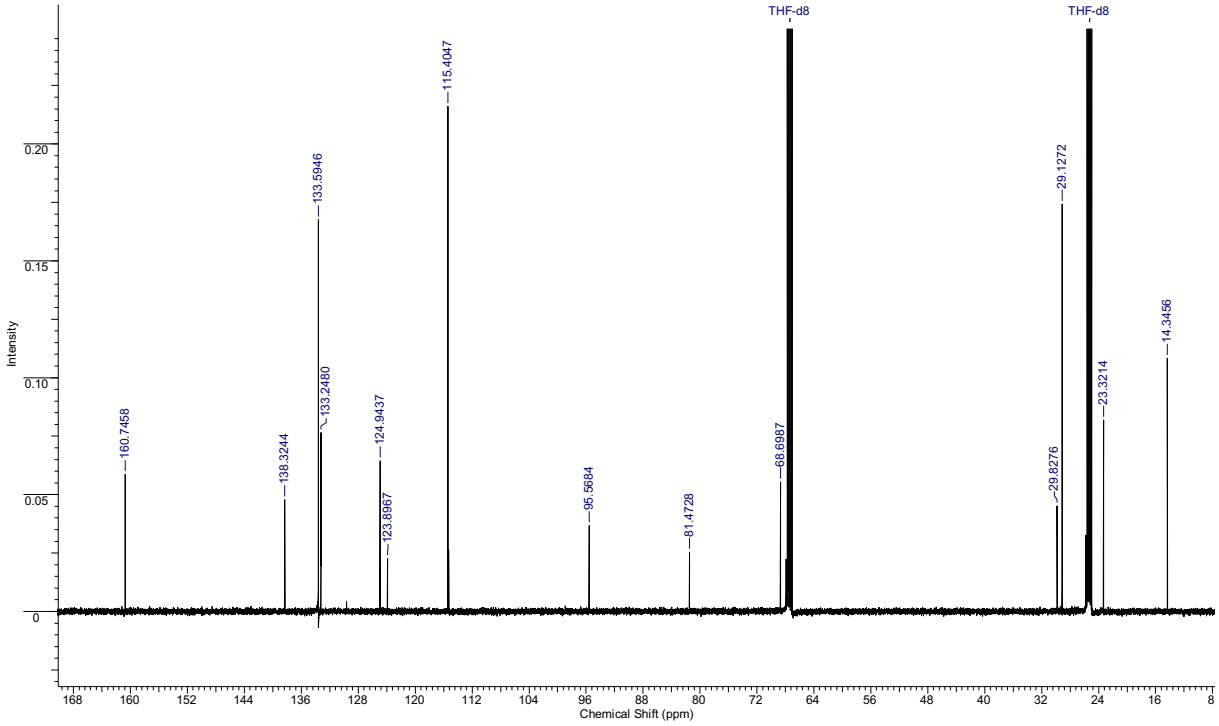

Figure S27. ^{13}C NMR spectrum of PET-5O (125 MHz, THF-d_8).

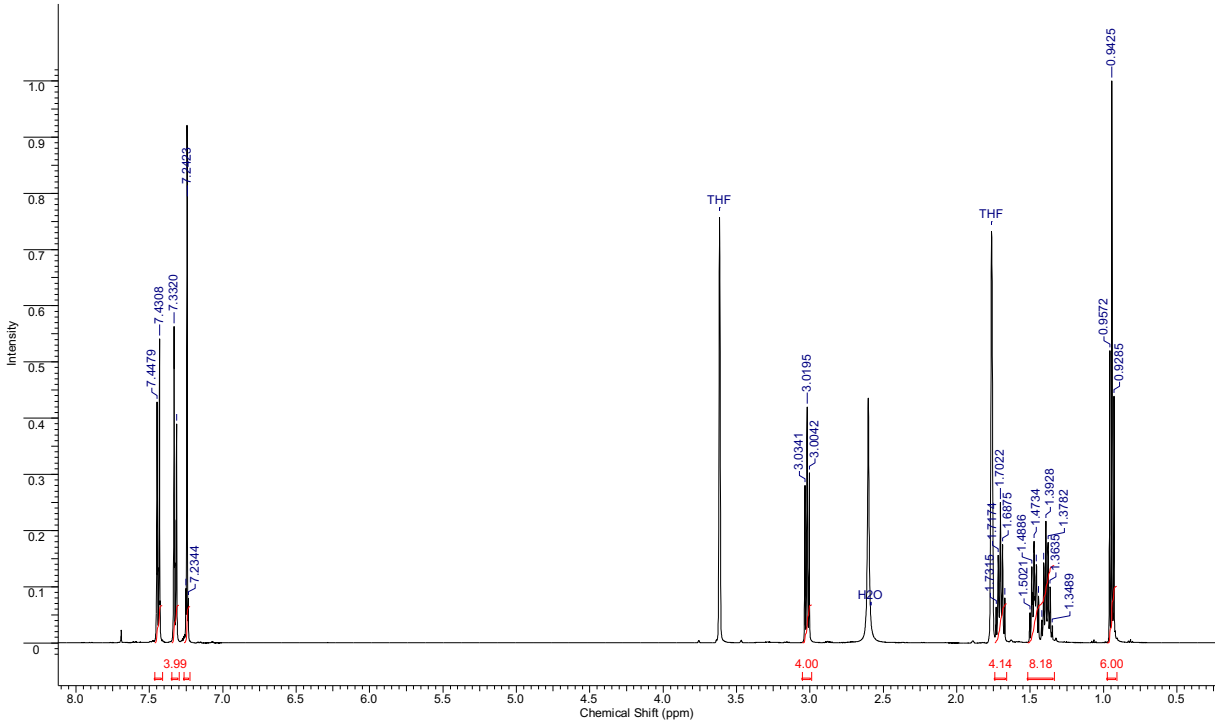

Figure S28. ^{1}H NMR spectrum of PET-5S (500MHz, THF-d_8).

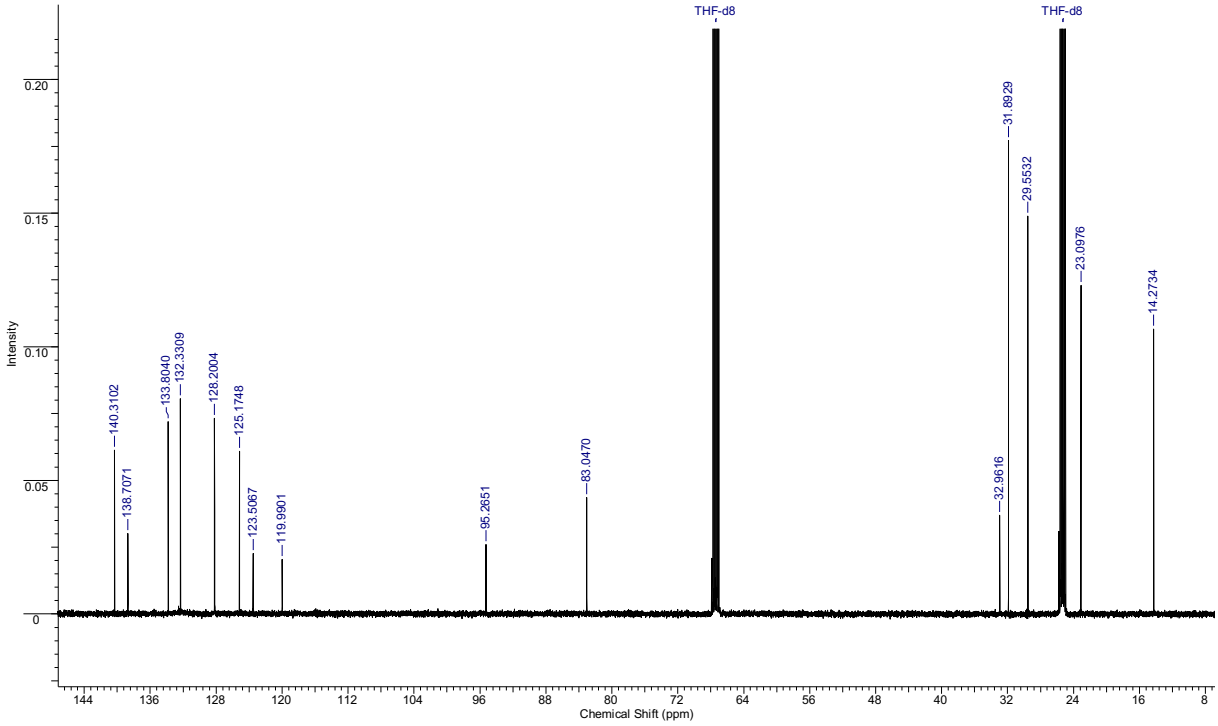

Figure S29. ^{13}C NMR spectrum of PET-5S (125 MHz, THF-d_8).

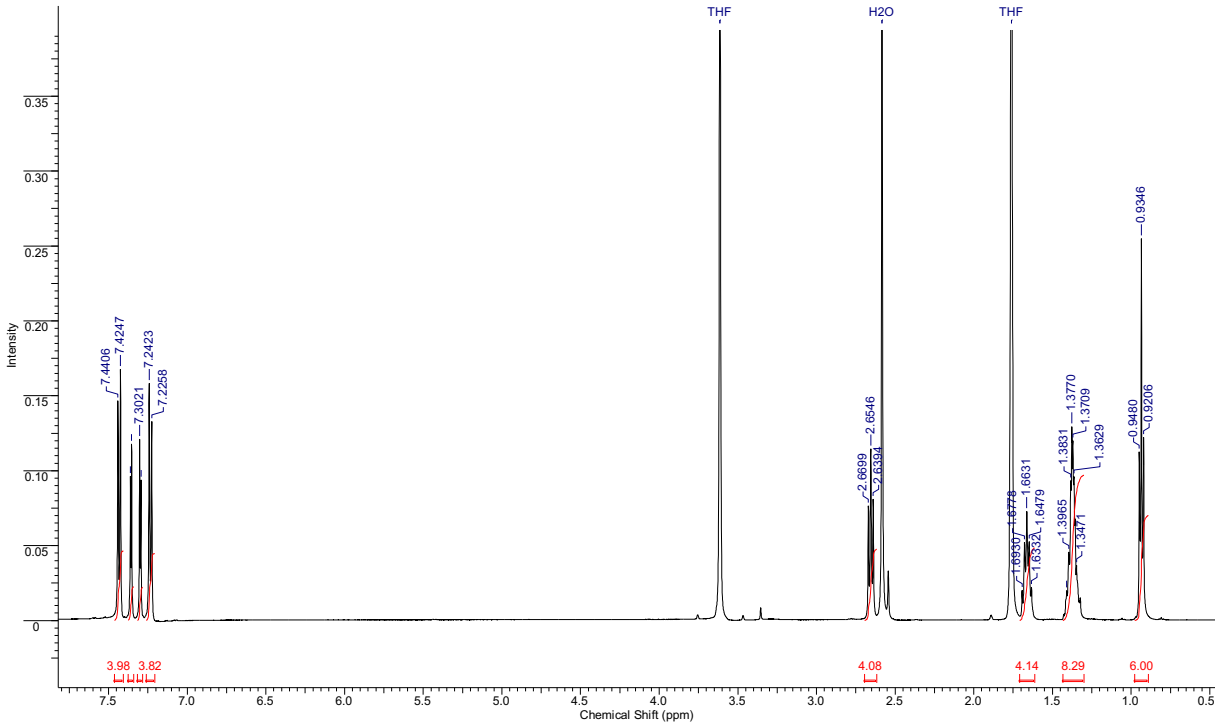

Figure S30. ^{1}H NMR spectrum of PES-5 (500MHz, THF-d_8).

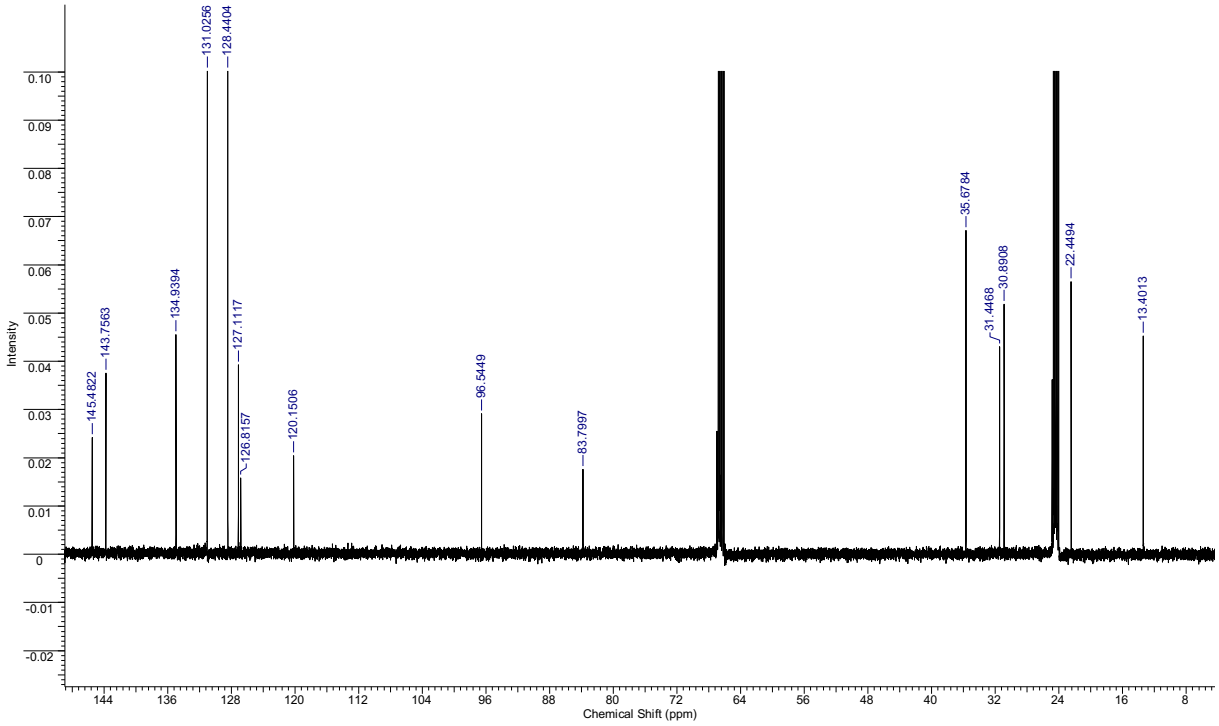

Figure S31. ^{13}C NMR spectrum of PES-5 (125 MHz, THF-d_8).

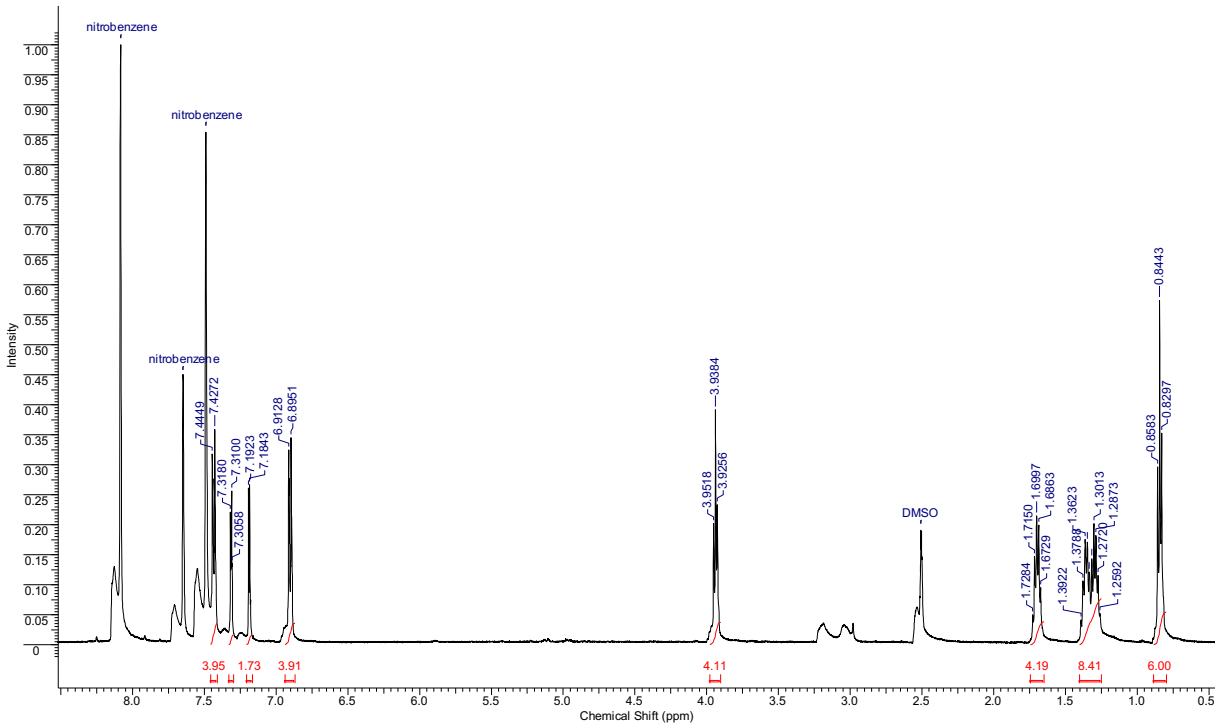

Figure S32. ^{1}H NMR spectrum of PES-5O (500 MHz, nitrobenzene-d_5/DMSO-d_6).

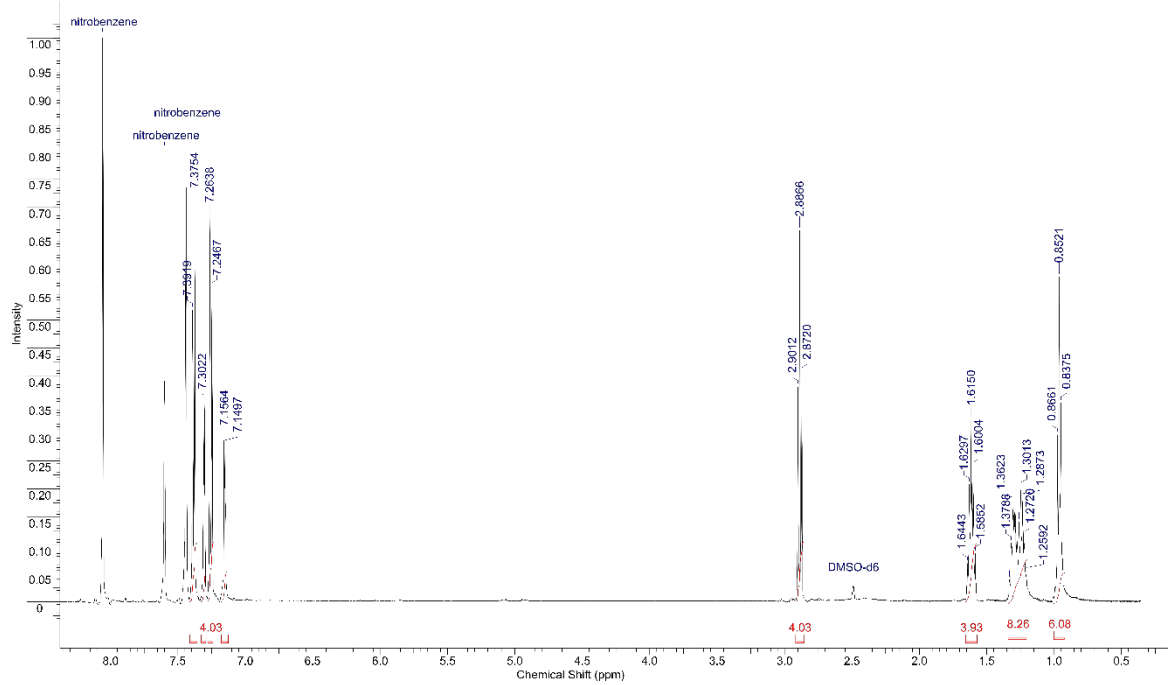

Figure S33. ^{1}H NMR spectrum of PES-5S (500 MHz, nitrobenzene-d_5/DMSO-d_6).

References

(1) Frisch, M. J.; Trucks, G. W.; Schlegel, H. B.; Scuseria, G. E.; Robb, M. A.; Cheeseman, J. R.; Scalmani, G.; Barone, V.; Petersson, G. A.; Nakatsuji, H.; Li, X.; Caricato, M.; Marenich, A. V; Bloino, J.; Janesko, B. G.; Gomperts, R.; Mennucci, B.; Hratchian, H. P.; Ortiz, J. V; Izmaylov, A. F.; Sonnenberg, J. L.; Williams; Ding, F.; Lipparini, F.; Egidi, F.; Goings, J.; Peng, B.; Petrone, A.; Henderson, T.; Ranasinghe, D.; Zakrzewski, V. G.; Gao, J.; Rega, N.; Zheng, G.; Liang, W.; Hada, M.; Ehara, M.; Toyota, K.; Fukuda, R.; Hasegawa, J.; Ishida, M.; Nakajima, T.; Honda, Y.; Kitao, O.; Nakai, H.; Vreven, T.; Throssell, K.; Montgomery Jr., J. A.; Peralta, J. E.; Ogliaro, F.; Bearpark, M. J.; Heyd, J. J.; Brothers, E. N.; Kudin, K. N.; Staroverov, V. N.; Keith, T. A.; Kobayashi, R.; Normand, J.; Raghavachari, K.; Rendell, A. P.; Burant, J. C.; Iyengar, S. S.; Tomasi, J.; Cossi, M.; Millam, J. M.; Klene, M.; Adamo, C.; Cammi, R.; Ochterski, J. W.; Martin, R. L.; Morokuma, K.; Farkas, O.; Foresman, J. B.; Fox, D. J. Gaussian 16 Rev. C.01. Wallingford, CT 2016.

(2) Yanai, T.; Tew, D. P.; Handy, N. C. A New Hybrid Exchange–Correlation Functional Using the Coulomb-Attenuating Method (CAM-B3LYP). *Chem Phys Lett* **2004**, *393* (1–3), 51–57. https://doi.org/10.1016/J.CPLETT.2004.06.011.

(3) Castet, F.; Champagne, B. Assessment of DFT Exchange-Correlation Functionals for Evaluating the Multipolar Contributions to the Quadratic Nonlinear Optical Responses of Small Reference Molecules. *J Chem Theory Comput* **2012**, *8* (6), 2044–2052. https://doi.org/10.1021/ct300174z.

(4) Aidas, K.; Angeli, C.; Bak, K. L.; Bakken, V.; Bast, R.; Boman, L.; Christiansen, O.; Cimiraglia, R.; Coriani, S.; Dahle, P.; Dalskov, E. K.; Ekström, U.; Enevoldsen, T.; Eriksen, J. J.; Ettenhuber, P.; Fernández, B.; Ferrighi, L.; Fliegl, H.; Frediani, L.; Hald, K.; Halkier, A.; Hättig, C.; Heiberg, H.; Helgaker, T.; Hennum, A. C.; Hettema, H.; Hjertenæs, E.; Høst, S.; Høyvik, I. M.; Iozzi, M. F.; Jansík, B.; Jensen, H. J. A.; Jonsson, D.; Jørgensen, P.; Kauczor, J.; Kirpekar, S.; Kjærgaard, T.; Klopper, W.; Knecht, S.; Kobayashi, R.; Koch, H.; Kongsted, J.; Krapp, A.; Kristensen, K.; Ligabue, A.; Lutnæs, O. B.; Melo, J. I.; Mikkelsen, K. V.; Myhre, R. H.; Neiss, C.; Nielsen, C. B.; Norman, P.; Olsen, J.; Olsen, J. M. H.; Osted, A.; Packer, M. J.; Pawlowski, F.; Pedersen, T. B.; Provasi, P. F.; Reine, S.; Rinkevicius, Z.; Ruden, T. A.; Ruud, K.; Rybkin, V. V.; Sałek, P.; Samson, C. C. M.; de Merás, A. S.; Saue, T.; Sauer, S. P. A.; Schimmelpfennig, B.; Sneskov, K.; Steindal, A. H.; Sylvester-Hvid, K. O.; Taylor, P. R.; Teale, A. M.; Tellgren, E. I.; Tew, D. P.; Thorvaldsen, A. J.; Thøgersen, L.; Vahtras, O.; Watson, M. A.; Wilson, D. J. D.; Ziolkowski, M.; Ågren, H. The Dalton Quantum Chemistry Program System. *Wiley Interdisciplinary Reviews: Computational Molecular Science* **2014**, *4* (3), 269–284. https://doi.org/10.1002/WCMS.1172.

(5) Dalton, a Molecular Electronic Structure Program. see http://daltonprogram.org 2022.

(6) Kubodera, K.; Kobayashi, H. Determination of Third-Order Nonlinear Optical Susceptibilities for Organic Materials by Third-Harmonic Generation. *Molecular Crystals and Liquid Crystals* **1990**, *182* (1), 103–113. https://doi.org/10.1080/00268949008047792.

(7) Egawa, K.; Gotoh, T.; Kondoh, T.; Kubodera, K. Exceptionally Large Third-Order Optical Nonlinearity of the Organic Charge-Transfer Complex. *JOSA B, Vol. 6, Issue 4, pp. 703-706* **1989**, *6* (4), 703–706. https://doi.org/10.1364/JOSAB.6.000703.

(8) Bass, M.; DeCusatis, C.; Li, G.; Mahajan, V. N.; Enoch, J.; Stryland, E. V; of America, O. S. *THIRD-ORDER OPTICAL NONLINEARITIES*; McGraw-Hill Education, 2010.

(9) Gubler, U.; Bosshard, C. Optical Third-Harmonic Generation of Fused Silica in Gas Atmosphere: Absolute Value of the Third-Order Nonlinear Optical Susceptibility X3. *Phys Rev B* **2000**, *61* (16), 10702–10710. https://doi.org/10.1103/PhysRevB.61.10702.